Nuclear Instruments and Methods in Physics Research A262 (1987) 463–495
North-Holland, Amsterdam

THE FRÉJUS NUCLEON DECAY DETECTOR

FRÉJUS COLLABORATION

Ch. BERGER, A. HOFMANN, H. MÖNCH, F. RAUPACH, P. SCHLEPER, G. SCHMITZ, J. TUTAS and B. VOIGTLÄNDER

*I. Physikalishes Institut der RWTH Aachen *, D-5100 Aachen, FRG*

C. ARPESELLA, Y. BENADJAL, Ph. BERNAUDIN, D. BLUM, C. BOURDARIOUS, J. BRUGNON, M. CORAZZI, G. DEUZET, B. DUDELZAK, P. ESCHSTRUTH, S. JULLIAN, D. LALANNE, F. LAPLANCHE, C. LONGUEMARE, C. PAULOT, A. REBOUX, Ph. ROY, J.L. SAURY and G. SZKLARZ

*Laboratoire de l'Accélérateur Linéaire **, Centre d'Orsay, Bâtiment 200, F-91405 Orsay, France*

L. BEHR, R.W. BLAND [+], F. BOUSSER, A. DEBRAINE, B. DEGRANGE, R. MARBOT, U. NGUYEN-KHAC, B. PIETRZYK [++], J. RAGUET [++], P. SERRI and S. TISSERANT

*LPNHE-Ecole Polytechnique **, Route de Saclay, F-91128 Palaiseau, France*

M. ARIGNON, M. ARNAUD, A. BARACAT, P. BAREYRE, R. BARLOUTAUD, R. BENAIT, A. BORG, G. CHARDIN, E. COULAREAU, L. DI CIACCIO [§], D. EDMUNDS [§§], J. ERNWEIN, G. GERBIER ***, J.F. GLICENSTEIN, J. HEITZMANN, M.A. JABIOL, M. JACQUET, W. KOLTON, Y. LAIGNEAU, C. MATHIS, L. MOSCA, L. MOSCOSO, P. PAILLER, S. PALANQUE, J. PELLE and B. TALLINI [†]

DPhPE-Saclay [+++], BP No. 2, F-91191 Gif-sur-Yvette, France

K.H. BECKER, H.J. DAUM, S. DENSKI, R. HINNERS, W. KOHRS, B. KUZNIK, R. MAYER, H. MEYER, D. ORTMANN, J. PETERS, M. SCHUBNELL, J. THIERJUNG, P. WINTGEN and Y. WEI

*Universität-Gesamthochschule Wuppertal *, D-5600 Wuppertal 1, FRG*

Received 1 July 1987

The characteristics, trigger and monitoring systems, data acquisition as well as the performance of the Fréjus nucleon decay detector are presented.

* Supported by the BMFT, FRG.

** Institut National de Physique Nucléaire et de Physique des Particules du CRNS.

[+] Permanent address: San Francisco State University, San Francisco, CA 94132, USA.

[++] Present address: Centre de Physique des Particules, F-13288 Marseille, France.

[§] Present address: Dipartimento di Fisica, Università di Roma II, Roma, Italy.

[§§] Permanent address: Michigan State University, East Lansing, MI 48824, USA.

*** Present address: LBL, Berkeley, CA 94720, USA.

[†] Deceased, 1981.

[+++] Institut de Recherche Fondamentale du CEA.

0168-9002/87/$03.50

1. Introduction

This paper describes the modular tracking calorimeter located in the Fréjus Underground Laboratory. This detector has been designed to study nucleon stability and cosmic-ray physics through the interaction of neutrinos and cosmic-ray muons. The physics motivations for this experiment can be found in ref. [1].

Nucleon decay detectors require three main qualities: a large mass to be sensitive to long lifetimes (~ 1 kt for 10^{32} yr), a high spatial resolution in order to identify and measure the low energy decay particles, and low noise. In the 900 t Fréjus detector, the spatial

resolution is ~ 5 mm and the noise smaller than one hit cell in a volume typical of a nucleon decay event (~ 1 m^3). Moreover, as this detector is made of Geiger tubes triggering flash chambers which have a few seconds dead time, the rate of atmospheric muons crossing the detector should be limited to about one per minute, in order to keep the total dead time small. On the other hand, the need for continuous monitoring of the detector requires at least a few muons per hour. The rock cover over the Fréjus Underground Laboratory is 1780 m on the average (4850 hg/cm^2) and is quite ideal for this kind of detector since the muon flux is 4.2 $m^{-2} d^{-1}$ and corresponds to ~ 20 muons crossing the detector per hour. The Fréjus highway tunnel, connecting France and Italy under the Alps, began operation in 1980. The Fréjus Underground Laboratory (fig. 1), located at the center of the Fréjus tunnel between Modane and Bardonecchia was excavated in 1982 and equipped with electric power, air conditioning and a steel structure to hold the detector. The volume of the laboratory is about 3500 m^3. Details on the Fréjus Underground Laboratory and equipment can be found in ref. [2]. The detector itself was built during 1983 and 1984 by a collaboration of five French and German laboratories: Aachen, Orsay, Palaiseau, Saclay and Wuppertal. The installation of the detector started in 1983 and ended in spring 1985. Data acquisition began in February 1984 when the detector mass reached 240 t, and continued while the mounting of the detector was in progress. The full 900 t detector was completed in June 1985.

The paper is divided as follows: in section 2, we describe the flash chambers and the Geiger tubes as well as their readout electronics. The trigger logic is explained in section 3, while the data acquisition and the monitoring of the detector are described in sections 4 and 5. Finally, in section 6, the performance of the detector is studied with respect to nucleon decay and cosmic-ray events. In particular, calibration studies made with a test detector of identical structure exposed to electron, pion and proton beams are presented.

2. Description of the detector

2.1. General description

The 900 t detector is made of a 912-layer sandwich of 3 mm thick iron plates and (5 mm × 5 mm) plastic

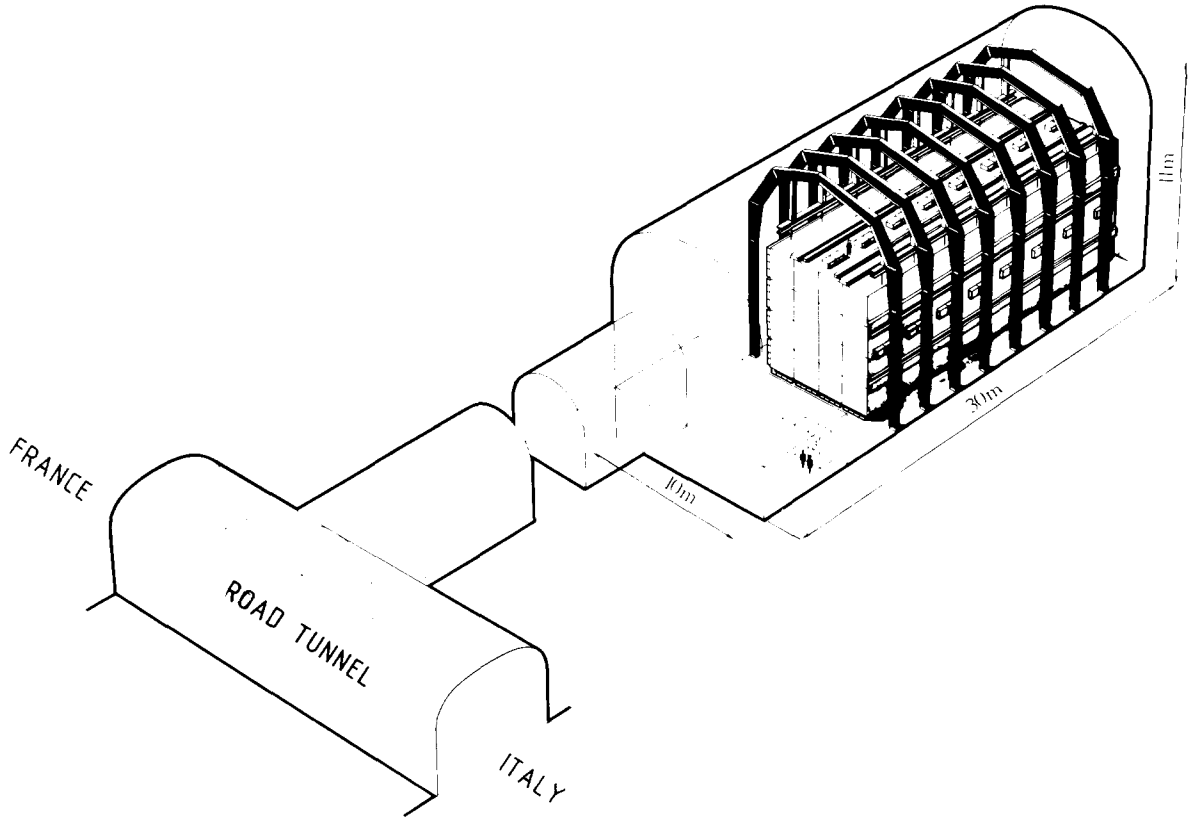

Fig. 1. The Fréjus underground laboratory.

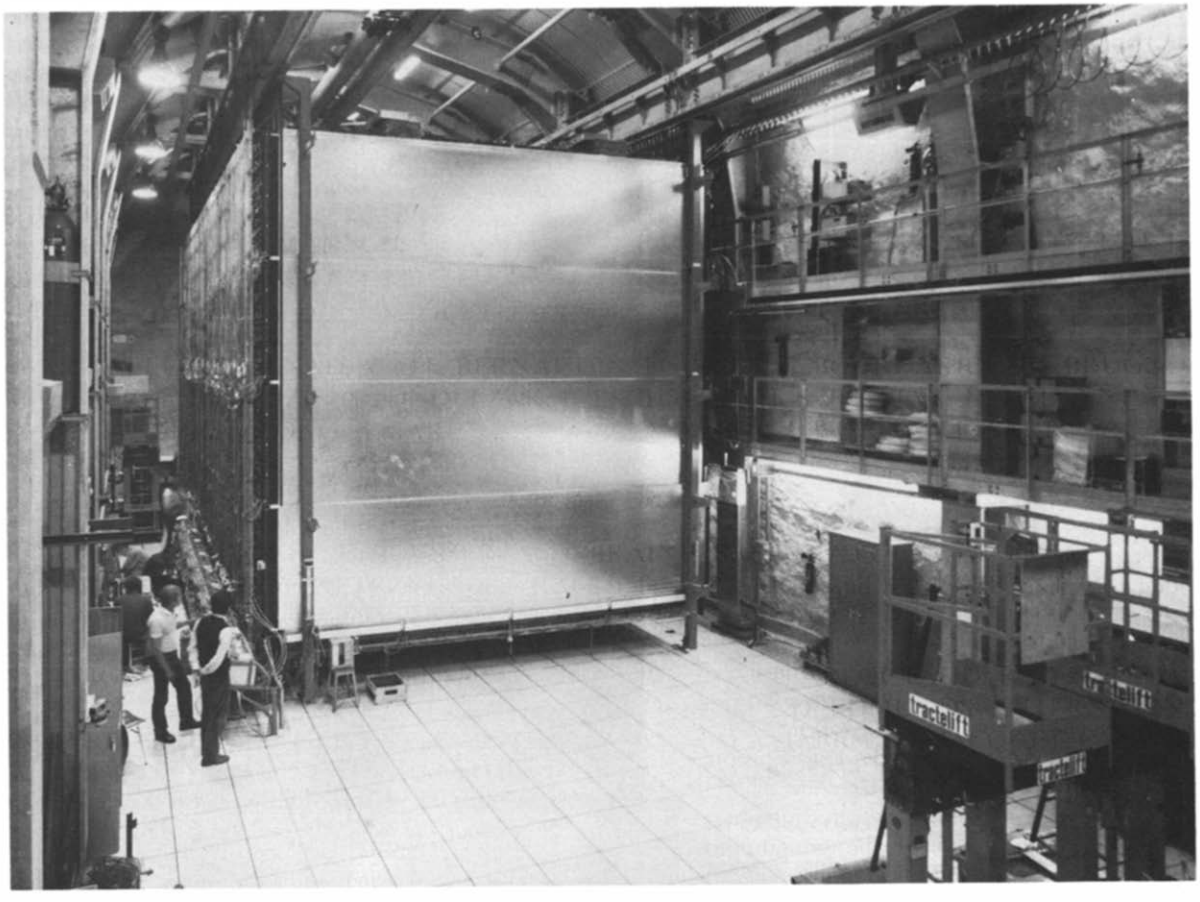

Fig. 2. General view of the detector.

flash tubes. The trigger for the flash chambers is provided by planes of Geiger tubes (15 mm × 15 mm in cross section) encountered every 8 flash chamber planes. A supermodule consists of 16 flash chamber planes and 2 Geiger planes. The detector, shown in fig. 2, is a parallelepiped (6 m × 6 m × 12.3 m) with an average density of 1.95 g/cm^3. The vertical iron and detector planes are hanging from a steel structure. A total of 33000 m^2 of polypropylene panels and 4000 m^2 of aluminum extrusions were used to build the detector. The detector tubes (Geiger and flash) are alternatively vertical and horizontal, and provide two orthogonal views (fig. 3). Therefore the flash chambers sample an event every 3 mm of iron (0.17 radiation length) whereas the sampling at the trigger level by the Geiger tubes is 24 mm of iron (1.45 radiation length). In principle, many detection techniques could have been used to build a 900 t fine grain tracking calorimeter. However, various constraints such as cost, long term reliability, maintenance, low noise, the need for mass production and the low muon flux in the underground laboratory guided the choices which were made. This one million channel detector made of Geiger tubes and flash chambers is of relatively modest cost because it uses inexpensive material such as iron, extruded aluminum and polypropylene plastic and because these detectors produce signals strong enough not to require amplification, and therefore make it possible to use inexpensive electronics. Also the large amount of detector elements which had to be built made it necessary to find industrial solutions to the technological problems which were encountered. The gases used in these detectors (argon in Geiger tubes, neon and helium in flash chambers) are nonflammable, which made them suitable for use in an underground laboratory.

2.2. Flash chambers

Following the development by Conversi et al. [3] of a simple and inexpensive way to build flash chambers, these detectors, which have a rather long recovery time (2–3 s), are being used in fine grain calorimeters built for experiments with very low event rates such as in neutrino experiments [4,5]. These detectors are charac-

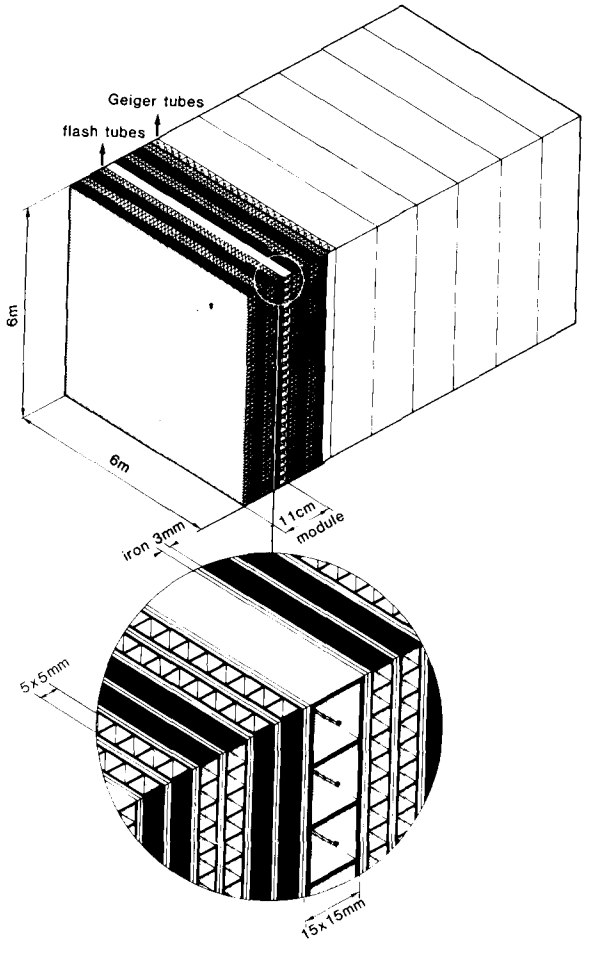

Fig. 3. Structure of the detector.

terized by an excellent pattern recognition capability, good energy and angular resolutions.

The operation of a large plastic flash chamber can be summarized as follows: a panel of extruded polypropylene is fitted with gas manifolds at both ends of its cells. This allows a mixture of neon–helium gas to flow through the chamber. Shortly after an ionizing particle has traversed the chamber, a high voltage pulse is applied to metal electrodes glued on both sides of the polypropylene panel. The intense field (~ 8 kV/cm) produces a local discharge which propagates by photo-ionization processes over the entire cell as long as the field is applied. The presence of a discharge in any cell can be detected by optical or electrical means.

2.2.1. Materials and construction

A flash chamber (FC) element weighs 0.5 t and is made of two extruded black polypropylene panels 6 m $\times$ 1.5 m in dimension, each sandwiched between two sheets of iron, 1.5 mm thick. All 256 cells in each panel are 6 m long and have a cross section of 5 mm $\times$ 5 mm. Fig. 4 shows the structure of an element. The large number of elements which had to be constructed (1850) over a period of two years made it necessary to reduce the number of manual operations during the assembly to a minimum. Therefore most items have been manufactured by industry to meet our needs and a special effort went into the design of specialized tooling.

The extrusion process [6] of the FC panels has been carefully monitored to ensure that the spacing of the cells is very regular in order to match the pitch of the readout strips. The amount of black coloring agent was permanently controlled because it is essential that flash chamber cells be optically independent to avoid flashover from one cell to its neighbors. To save time during assembly, the 50 μm thick aluminum foils were automatically glued on both sides of the panels during the extrusion process. The gas manifolds [7], made of a solid structure of molded polypropylene, are used to evenly distribute the gas among the cells. They also serve as a support for the readout printed circuit boards and the high voltage pulser. The 1.5 mm thick iron sheets are galvanized to prevent oxidation.

The main steps of the assembly which took place in a 1500 m^2 workshop can be summarized as follows. The polypropylene panels and the aluminum electrodes are cut to the required dimensions. The gas manifolds are fitted with black plastic foam [5,8] which absorbs the light from the plasma and thus suppresses flashover at the ends of the cells. The manifolds are then welded to the ends of the panel with a welding machine using a hot wire wrapped in kapton. Very good seals were obtained with this simple method. The total length of the welded seals is 22 km. Welding has been preferred to gluing because one would have to fear contamination of the gas by outgassing of the glue and because of long term reliability. The polypropylene panels, the iron sheets as well as the high voltage delay line are stacked as shown in fig. 5. It was found necessary to glue together the panels and the iron sheets to ensure the mechanical rigidity of the large multilayered structure of a 6 m $\times$ 6 m FC biplane when it is in the vertical position. The printed circuit board providing the connections between the delay line, the chamber electrodes and the hv pulser is then mounted. Finally the two external iron sheets are riveted together across two pieces of extruded aluminum of special shape. The completed FC elements are stacked into a test bench where their performance is checked with cosmic rays. They are then shipped by truck to the laboratory in the Fréjus tunnel. There, four elements are assembled into a 6 m $\times$ 6 m biplane hanging from a steel structure (figs. 1 and 2). At the design stage, a special effort went into reducing the dead space needed for assembly of two adjacent elements. It is very small: 5 cm (or 10 cells).

Not included prototype building and testing, the construction and assembly of the 900 detector lasted

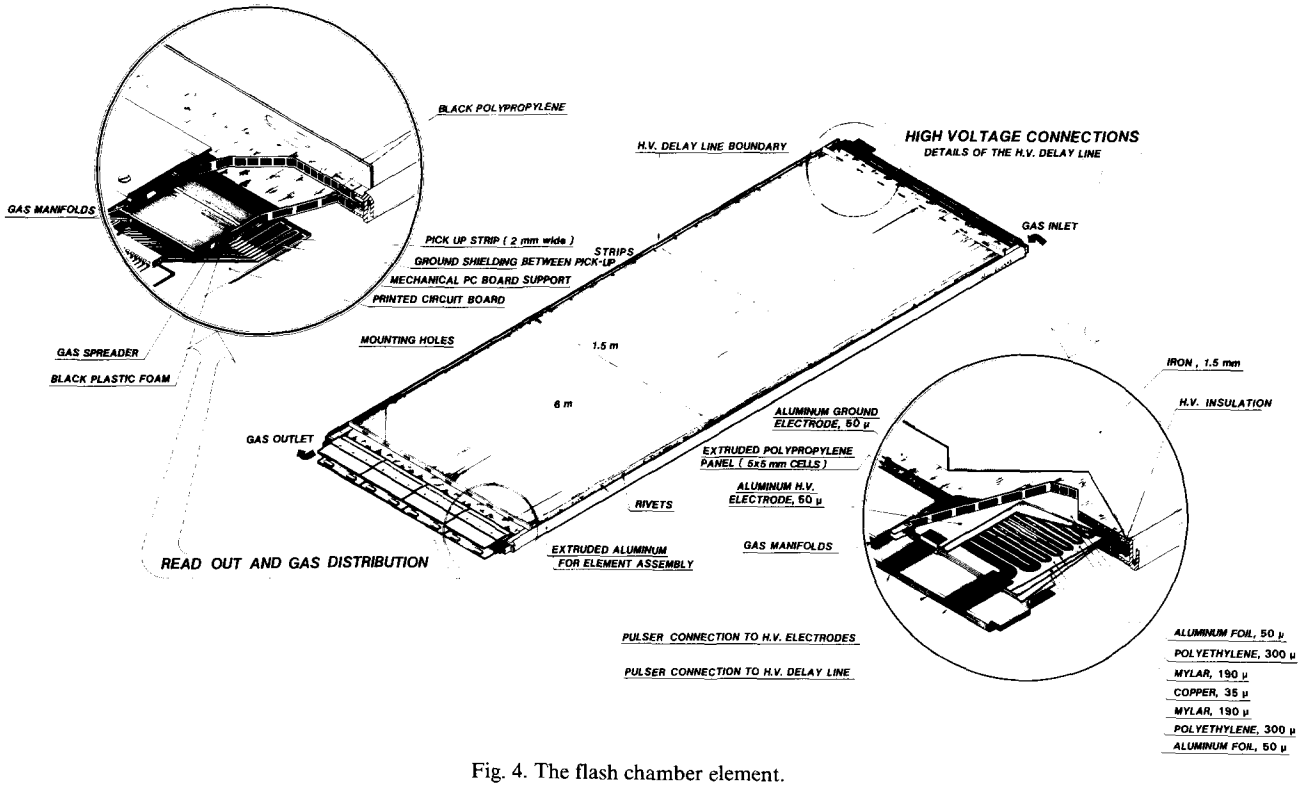

Fig. 4. The flash chamber element.

two years. More details on the FC construction can be found in ref. [9].

2.2.2. Gas distribution and purification

The FC gas most commonly used is neon because of its high yield of primary ionization when traversed by a charged particle and its high Townsend coefficient which ensures strong electron multiplication when the electrical field is applied. Because of its reduced cost, we use a mixture of 70% neon and 30% helium.

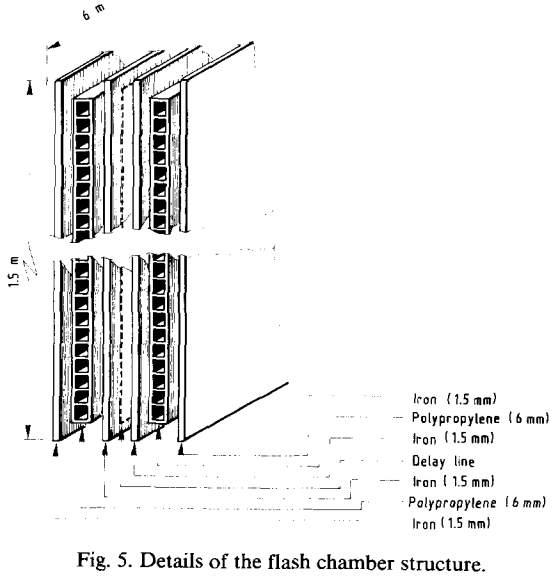

Fig. 5. Details of the flash chamber structure.

In order to reduce diffusion of FC gas to the outside and air to the inside through the plastic walls of the panels, we chose a rather large thickness of the external walls (0.5 mm). Furthermore the aluminum foils which are glued tightly to the two faces provide an additional barrier. Nonetheless, air diffuses to the inside of the panels through the aluminum-free areas and miniature pinholes. Outgassing from the polypropylene itself produces additional poisoning of the gas by various hydrocarbons. We tested two varieties of polypropylene and chose the one with the least outgassing [10]. Gas purity affects the properties of the flash chambers in several ways. During the time between the passage of the particle and the onset of the hv, the impurities tend to attach ionization electrons so that fewer of them are available for multiplication when the electrical field is applied. This results in a loss of efficiency and sensitive time (section 2.2.7). On the other hand, electronegative impurities are needed to favour recombination of the plasma. However, because of the low trigger rate (< 1 min^{-1}), reignition of hit cells is not a problem in this detector.

The FC gas is being purified and recirculated by a purification system (fig. 6) which uses two sets of

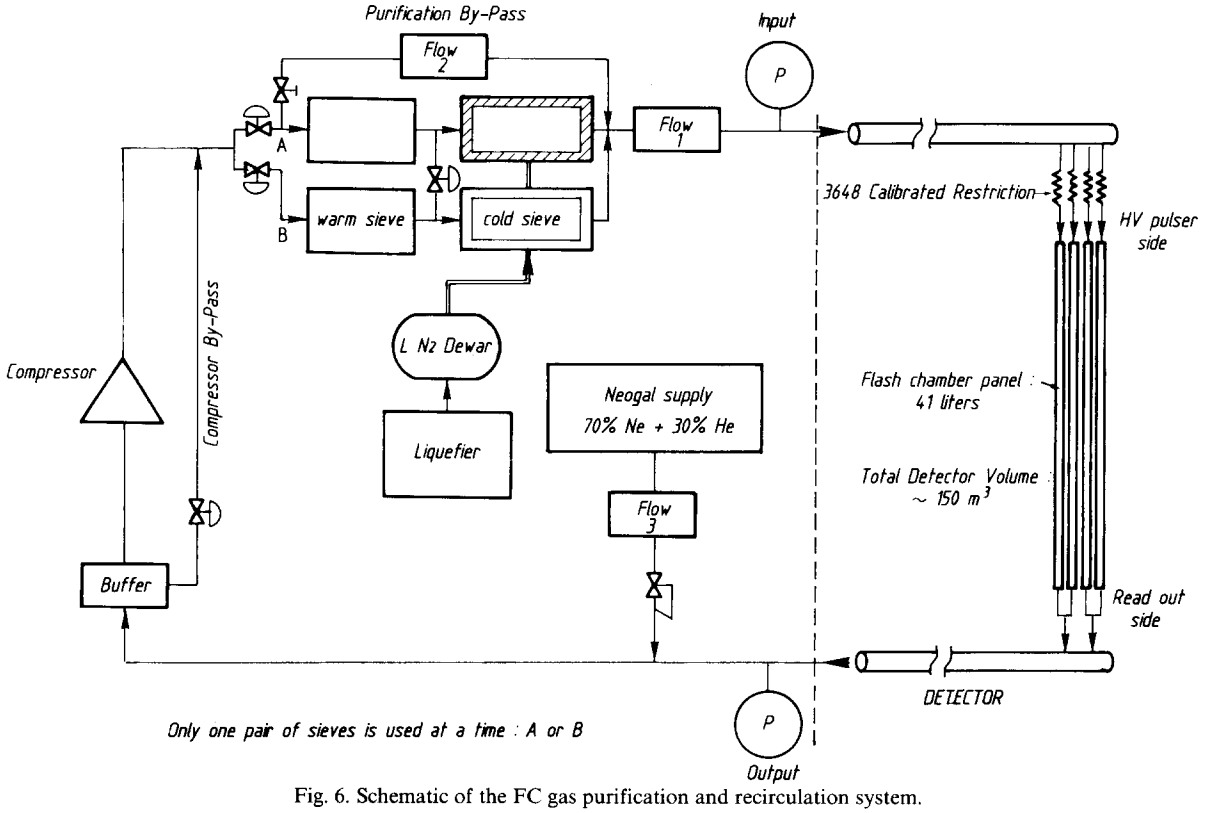

Fig. 6. Schematic of the FC gas purification and recirculation system.

molecular sieves. The first, at room temperature, removes water, the second, at liquid nitrogen temperature, removes oxygen, nitrogen and other gaseous impurities. The system is a scaled-up version of existing purifiers [11]. Its originality lies in its size (the flow rate can go up to 2 detector volumes per hour or 300 m^3/h), its totally automated operation [12] and its liquefier capable of producing 9 l/h of liquid nitrogen inside the laboratory [13]. The level of impurities in the flash chambers can be controlled by an adjustable bypass to the molecular sieves, by varying the cold sieve temperature or by the flow rate through the detector. It was found that with 200–400 ppm of oxygen and 50–150 ppm of nitrogen, as measured by a thermal conductivity gas chromatograph [14], adequate efficiency, sensitive time and reignition probability can be achieved.

When the molecular sieves become saturated after ~ 20 d of operation, the system is switched to the second set of sieves while the first one is being cleaned by pumping and heating in a regeneration process which lasts ~ 3 d.

For uniform response of the detector, it is necessary for each one of the ~ 10^6 cells to receive the same gas flow. At the opposite end of the readout region each panel of 256 cells is fed at constant pressure through a calibrated restriction whose impedance to the gas flow is much larger than the impedance of the panel itself (fig. 6). This ensures equal gas sharing among all panels. Inside the gas manifold, there is a metal gas spreader with 0.5 mm diameter holes every 3 mm. The gas enters and exits at diagonally opposite ends of the panel (fig. 4) so that the total path length through the manifolds and the cell is identical for each cell.

The pressure inside the panels is kept as low as possible to minimize gas leaks: at 2 mbar overpressure, the total leak rate is ~ 350 l/h or ~ 2.5×10^{-3} of the detector volume, two thirds of which occurs in the detector and the rest in the purification system. The cost of the FC gas is a substantial part of the running cost of the experiment.

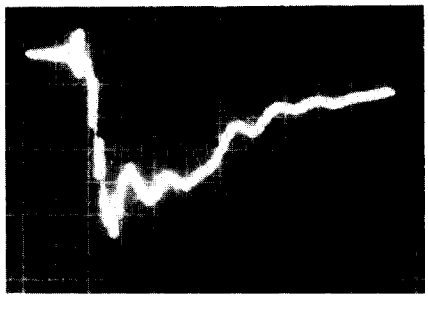

Fig. 7. The high voltage pulse: 1 kV/div., 200 ns/div.

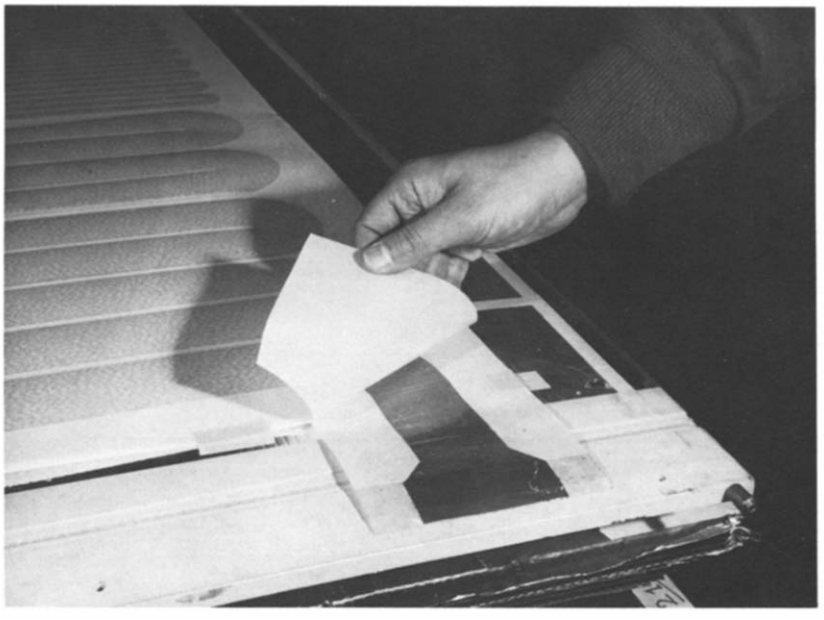

Fig. 8. The hv delay line.

2.2.3. High voltage

To achieve good efficiency over the entire area of the flash chamber, the high voltage (hv) pulse must have ~ 5 kV in amplitude, a rise time of < 100 ns and a duration of ≥ 800 ns (fig. 7). A short rise time is necessary to initiate the plasma discharge, because before reaching 3 kV, the hv acts as a clearing field for the ionization electrons. The duration of the hv pulse is critical in sustaining the plasma discharge long enough for it to propagate down the 6 m long cell to the readout region.

The hv pulse is produced by discharging a flat "zig-zag" delay line through a spark gap to the chamber electrodes. The 70 m long, 1.5 cm wide delay line [15] is made of a copper ribbon, 35 μm thick, sandwiched between sheets of insulator, 500 μm thick, and aluminum sheets on the outsides (figs. 4 and 8). The characteristic impedance of the line is $R_c = 4.2\ \Omega$ and the capacitance $C_L = 100$ nF. The first 6 m of the line are wider (5 cm) with $R_c = 1.25\ \Omega$ to produce the fast rise time [16]. The switching spark gap uses a spark plug (Champion N 19 V) and a stainless steel bolt with a tungsten cap. Both are mounted in a cylindrical plastic frame. The spark gap is operated in nitrogen at 300 mbar overpressure.

The delay line was preferred to capacitor banks because of its lower cost and because it could be embedded inside the FC biplane element, thus saving much space. The spark gap is mounted inside a plastic case, called a "pulser", along with charging and adapting resistors, and a pickup network for monitoring of the hv signal (fig. 9). One pulser is connected to two FC elements as shown in fig. 10. Each pulser is surrounded by a copper shield to prevent the spark gap electromagnetic noise from disturbing the electronics. There are a total of 912 pulsers which are removable for maintenance of the spark gaps.

The dc hv applied to the 1824 delay lines is provided by two computer controlled hv power supplies (9 kV, 3.5 A peak current) [17] through a resistor network which was chosen in such a way that 3 s after the trigger has produced the discharge, the delay lines are recharged at 99.9% of the nominal 7.5 kV value.

The pulse necessary to trigger the spark gaps is obtained by three thyratrons [18] which amplify the NIM signal from the trigger electronics to a hv pulse of amplitude 7 kV and rise time 20 ns. The total delay between the passage of an ionizing particle in the flash chambers and the presence of the hv on the FC electrodes is ~ 1.3 μs with three contributions: trigger electronics, hv amplification and signal transit time in cables.

2.2.4. Flash chamber readout

Electronic readout of the flash chamber information is used for this experiment. The discharge of a flash chamber cell is coupled to the readout electronics by metal strips positioned on top of each cell. An acceptable signal to crosstalk ratio is obtained because of the equal spacing of the cells, and a calibrated positioning of the readout boards during the assembly of the FC elements.

The pickup strips are 2 mm wide and 25 mm long. The distance to the ground foil is 2 mm. The uniformity of this distance, essential for equal pulse heights, is

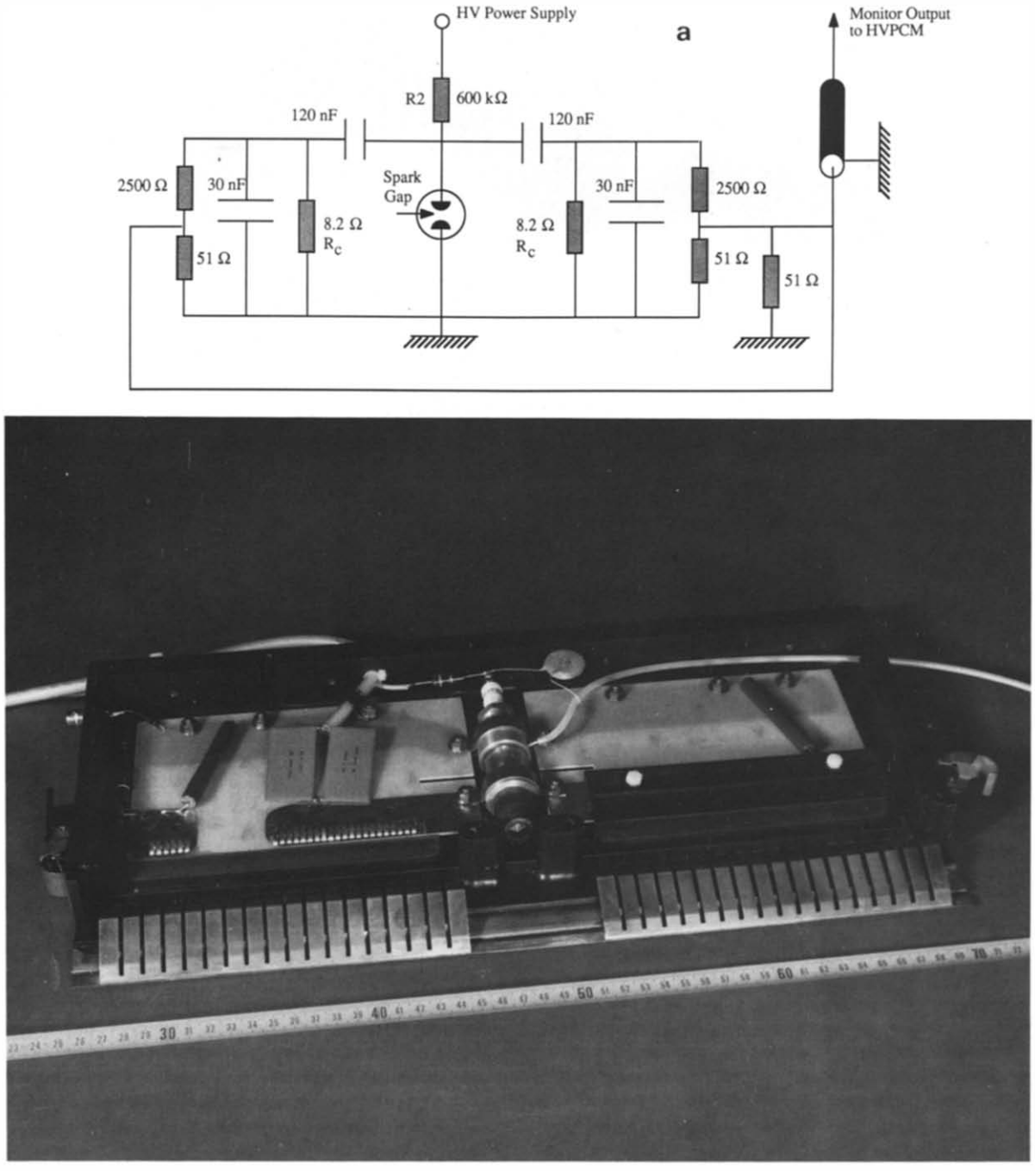

Fig. 9. (a) Schematic electrical diagram of the hv pulser. (b) Physical layout of the hv pulser.

ensured by a ground strip printed on the readout board which defines the end of the flash chamber ground. Ground strips placed between the pickup strips reduce the crosstalk between adjacent cells. The ground of the readout board is completely separated from the FC ground to avoid grounding problems. Fig. 11 shows the mechanical coupling of the readout board to the flash chamber element with the gas manifolds serving as a support.

The input circuit for the readout of an individual flash chamber cell is shown in fig. 12. A printed capacitor of 7 pF using the dead space on the printed circuit board reduces the peak voltage of the charge signal. The signal is fed through a resistive dividing network to a

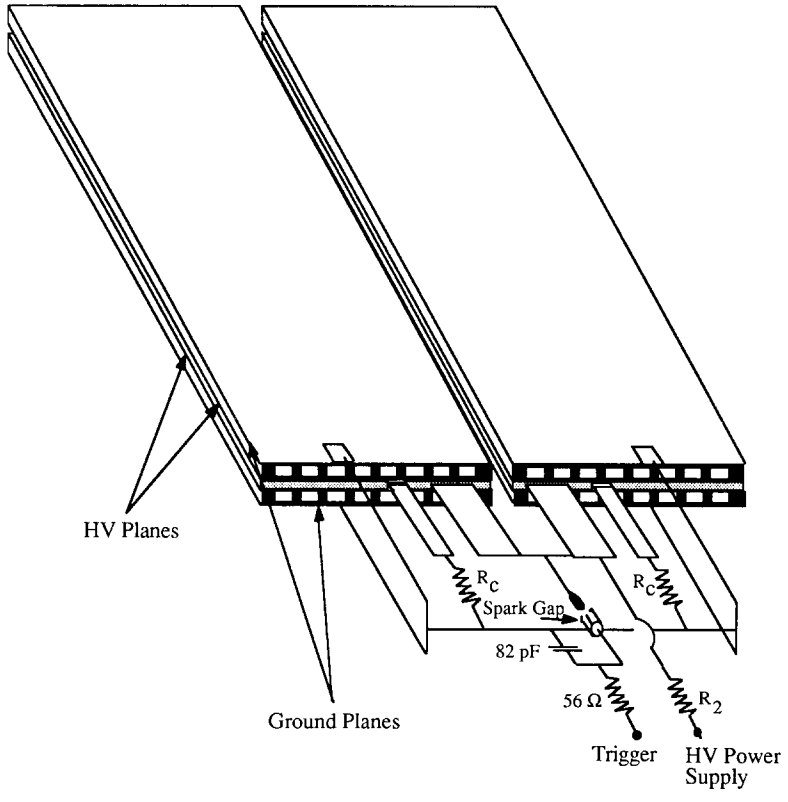

Fig. 10. Connection of the pulser to two FC elements.

parallel input of a CMOS shift register. The CMOS circuits operate at 12 V in order to be fast enough to use the CAMAC S1 pulse for deriving the shift register control signals, i.e. the load and the clock pulse. The flash chamber information is latched by a load signal derived from the trigger within about 1.5 μs after applying the high voltage to the flash chambers. The sensitivity of the shift registers can be varied by the offset voltage at the pedestal terminal and by the timing of the load signal with respect to the leading edge of the hv

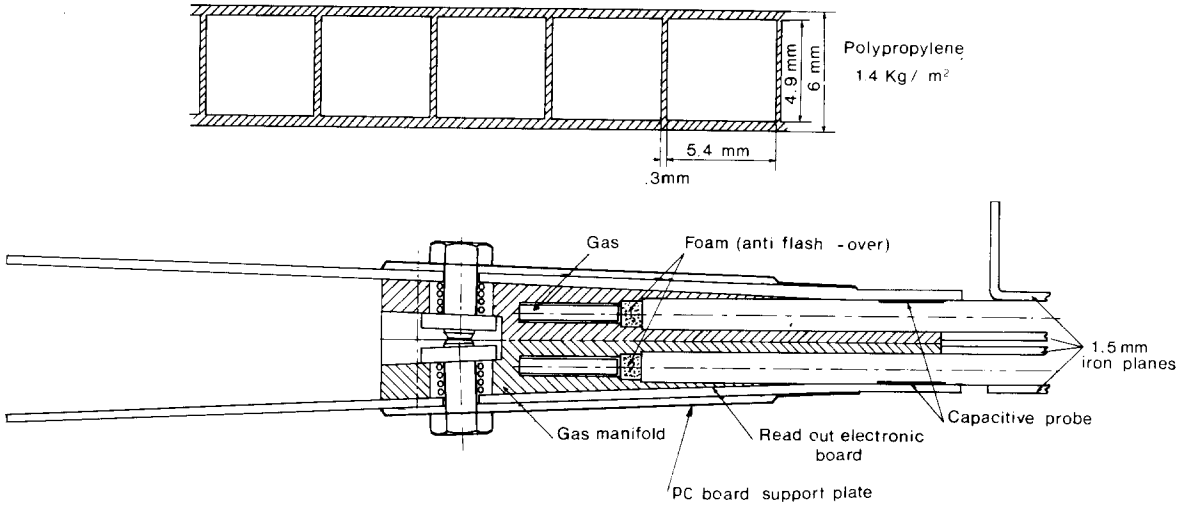

Fig. 11. Mechanical layout of the readout region.

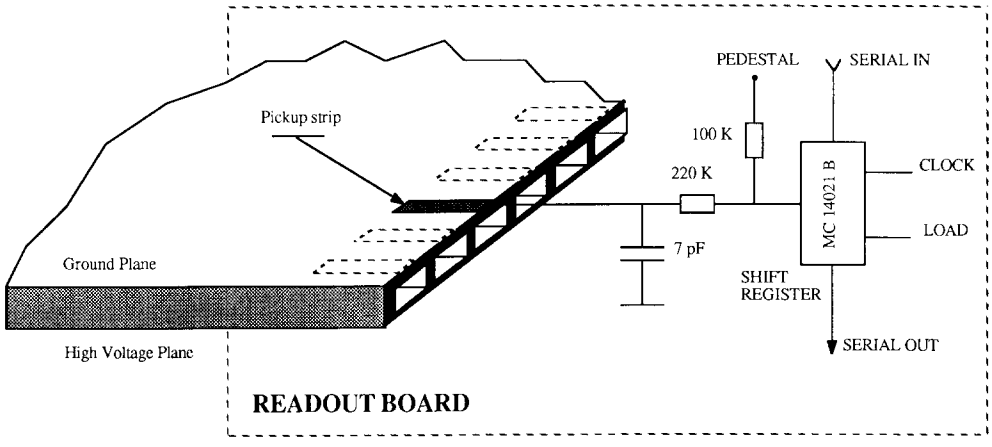

Fig. 12. The input circuit of the flash chamber readout.

pulse. In order to ensure uniform cell efficiency throughout the detector, the pedestal values can be tuned separately for each of the 1824 flash chamber elements. These values are defined on a disk file and can be modified on request. The pedestals are set by means of digital-to-analog converters located on a special "pedestal board". Two CAMAC boards are used to transmit the required voltage values from the computer to the "pedestal boards".

The flash chamber signal is shown in fig. 13. At an operating voltage of 7.5 kV, the total charge coupled to the pickup is of the order of 2 nC which is sufficient to drive high impedance logic devices without amplification. The signal of the discharge of a flash chamber is about 4 times larger than the crosstalk signal.

The schematics of the complete flash chamber readout system is depicted in fig. 14. A mixture of serial and parallel data processing is chosen to minimize the cabling, thus reducing costs and increasing the reliability of the system. The parallel data processing shortens the readout time and simplifies data reduction. The basic unit in this scheme is given by a single flash chamber panel which is read by one shift register chain consisting of 4 readout boards with 64 channels each. The shift registers may operate in a cyclic or in a serial-in serial-out mode. The two panels of a flash chamber element are equipped with two different versions of readout boards. Thus data are shifted in the same direction and no further data inversion is needed.

The 4 horizontal and 4 vertical FC elements of a biplane are controlled by one multiplexer board corresponding to 4096 flash chamber cells. The signal lines between the shift registers and the multiplexers consist of twisted pairs terminated with 110 Ω. The control signal for the CMOS shift registers are 12 V in amplitude thus ensuring worst case noise immunity of 90

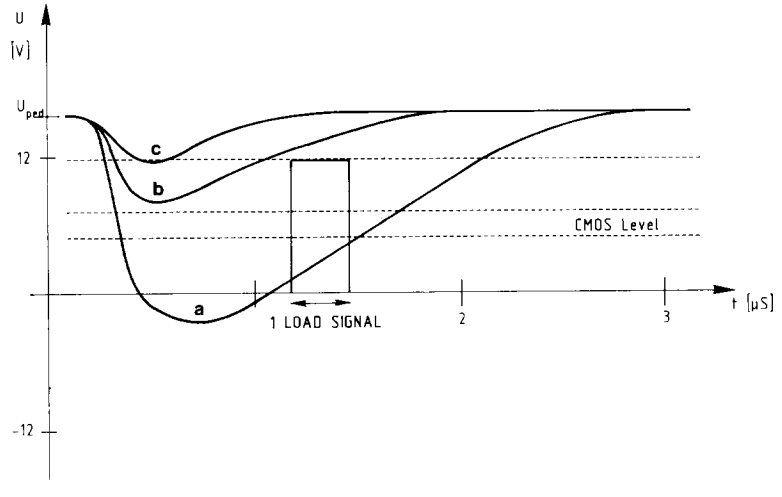

Fig. 13. The flash chamber signal: (a) direct signal, (b) crosstalk, (c) hv pickup.

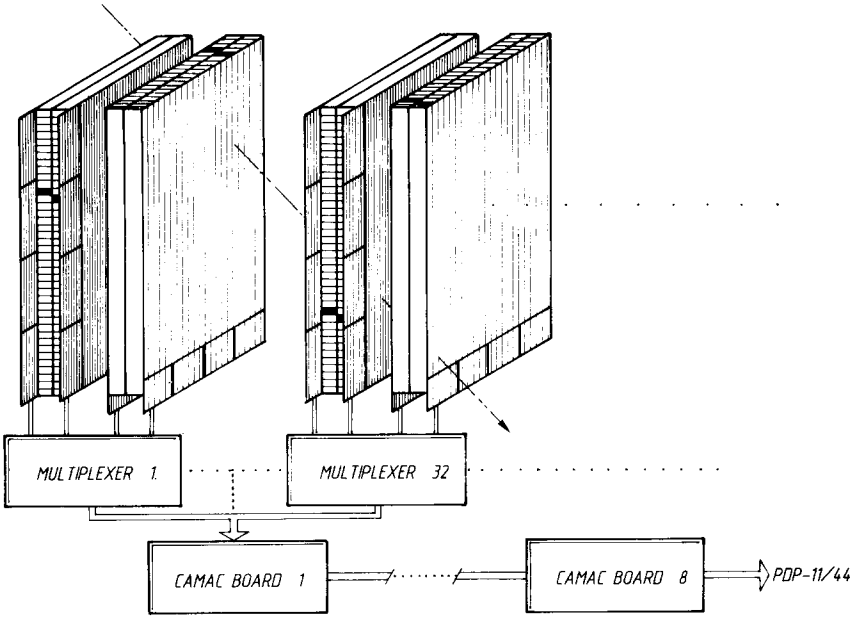

Fig. 14. Schematic of the flash chamber readout system.

mW. This high noise immunity completely eliminates the generation of spurious control signals on these lines during the the flash chamber hv pulse. The multiplexer board contains the logic necessary to read the flash chamber information, i.e. data multiplexers, clock demultiplexer, clock and load signal amplifiers as well as test facilities of the whole readout system as described in section 2.2.5. It also includes a voltage follower needed for setting different pedestals to each element's readout. The readout may be set in four different modes via the multiplexer boards. One of these modes is the normal readout mode while the remaining modes are used for testing the system.

The multiplexers are bussed in groups of 32 to one CAMAC readout board which controls the readout of 128 K cells. Eight of these CAMAC boards are sufficient to read all the flash chamber information of the 900 t detector. The CAMAC board sends the commands necessary for reading or testing the system to the 32 multiplexers in parallel and receives their response on 64 data lines and one control line. Through this line, it controls the cabling and generates error conditions if errors are detected as described in section 2.2.5.

The common mode rejection of the receivers on the multiplexer boards is not sufficient with such a large number of hv pulsers to avoid parasitic load and clock signals from being picked up on the cables which connect the multiplexer with the CAMAC system. An inhibit board inserted into the command bus near the multiplexers disables the load and command lines for several hundred ms when a trigger occurs. The load signal needed to latch the FC information is derived on this board from the trigger.

2.2.5. Flash chamber readout control

Several test and control facilities are implemented into the flash chamber readout system and are necessary to keep track of proper operation, to correct the data for spurious noise on the shift register command signals and to locate precisely electric failures.

Two of the test modes set by the multiplexer concern tests on the proper operation of the parallel inputs of the shift registers while the third test mode allows us to test the addressing of the multiplexers. These tests set the pedestal either to a high or low level for even and odd addressed cells or vice versa. Two tests are necessary to diagnose damage of an input circuit. The fact that the assignment of the tests is commuted for the two different versions of shift register boards used facilitates the tests of correct cabling within a FC plane.

The addressing of the multiplexers is checked by setting the shift registers to the serial-in serial-out mode. For each different multiplexer address, different bit patterns are written to the shift registers. This information is read subsequently. Deviations from the original data allow detection of addressing failures.

The clock pulse used to shift out the data is returned from the far end of the shift register chain and is used to generate a busy signal on the multiplexers. The busy signal starts upon receiving the leading edge of the clock signal from the CAMAC board and is terminated by the trailing edge of the clock returns of the two shift

register chains addressed in parallel by the multiplexer. The busy signals of the 32 multiplexers are controlled by one CAMAC readout board "wire-anded" on the command bus. On the front end multiplexer this information is used to generate a busy signal sent to the CAMAC readout board.

If the clock return signal of at least one of the 32 multiplexers is missing, the busy bus remains in the false state and the front end multiplexer generates a short pulse of opposite polarity with respect to the normal situation. The timing and the polarity of the busy signal are used on the CAMAC readout board to generate essentially two types of error conditions, i.e. "no busy signal received" and "wrong busy signal received". By means of the busy signal, the cabling, the power supplies and the proper operation of the whole readout system are controlled at each clock pulse.

In addition to the busy system which monitors the hardware of the readout, a second control system is implemented on the flash chamber readout boards to detect spurious signals on the load and clock lines due to flashing the detector and controls the hardware as well. To be able to detect noise pulses on the shift register command lines, fixed fiducial patterns are incorporated in the shift register chain on each readout board. Groups of 64 bits of data are followed by an 8-bit fiducial word constructed in such a way as to detect up to four wrong shifts in either direction or to signal severe data losses or malfunctioning of the readout if it is impossible to retrieve the bit pattern.

If fiducial or busy errors are encountered during the readout procedure the error information is recorded with the events and appears on an on-line error log. By using test and debugging programs the reason for the error condition can be easily located.

2.2.6. Performance of the flash chamber readout

About 15000 FC readout boards are needed to read the entire detector. To avoid frequent replacement of readout boards, a burn-in is performed with all shift register readout boards after assembly. The boards were operated for one week at an ambient temperature of 80 °C at 12 V in a cyclic readout mode with a clock frequency of 1 MHz. This procedure is equivalent to a one year normal operation and totally prevents failures due to "infant mortality" of the electronics. The failure rate of the readout boards during three years of operation is found to be less than 0.05% per year and corresponds to the expected rate.

The data integrity is monitored by the fiducial mark system as explained above. The average fiducial error rate is $\sim 10^{-5}$ per event and corresponds to a 1% probability of having a wrong shift in a normal event because of the hv pulser noise.

To obtain good uniformity of the plasma pulse height, only $\sim 15\%$ of the FC elements need pedestal values different from the standard setting.

2.2.7. Flash chamber performance

It is very difficult to determine the fundamental physical parameters which govern the functioning of flash chambers, i.e. the primary ionization produced by a minimum ionizing particle, the Townsend coefficient and the mean free path of an electron in the gas before attachment. They are obscured by the many parameters which influence the performance of this flash chamber detector. The most important ones are: the characteristics of the hv pulse (amplitude, rise time, delay) and the gas purity.

These parameters often have opposite effects on the flash chamber properties and their values are usually the result of a compromise. As an illustration, optimum efficiency would require a hv value incompatible with a low number of noisy cells and with a long lifetime of the hv pulsers. In the same way, very pure gas which is desirable for good efficiency is unsuited for low reignition probability.

The efficiency of the flash chambers is continuously monitored by analyzing muons crossing the detector without visible bremsstrahlung. For each muon the efficiency ϵ of a panel is defined as:

$$\epsilon = N_{\text{hits}}/\alpha(1 + \operatorname{cotg}\,\theta), \tag{1}$$

where N_{hits} is the number of hits in the panel belonging to the fitted straight track, α is the ratio of the active to the total cell width and θ the angle between the muon track and the panel (fig. 15).

The average efficiency of all flash chambers is shown in fig. 16 as a function of the amplitude of the hv pulse. The smooth rather than steep rise of the efficiency reflects the fact that it is the average efficiency for all 3648 panels which is shown. Panels have slightly different plateau heights and thresholds. At the chosen 7.5 kV setting of the power supply, which corresponds to a 5 kV pulse, and for standard gas conditions, the distribution of panel efficiencies has an average value of 86% and a σ of 20%.

The efficiency is also dependent on the delay between the particle crossing and the onset of the hv pulse on the chambers. Diffusion of the ionization electrons in the gas and attachment by electronegative impurities decrease the number of electrons available for initiating an avalanche. This effect results in lower efficiency as the hv delay increases (fig. 17). The delay has been set to the minimum possible value of 1.3 μs.

As expected, the efficiency depends on the particle direction with respect to the chamber planes because the primary ionization is proportional to the distance travelled by the ionizing particle in the gas (fig. 15). The variation of the efficiency as a function of the track length in the FC cell is shown in fig. 18. From this, one

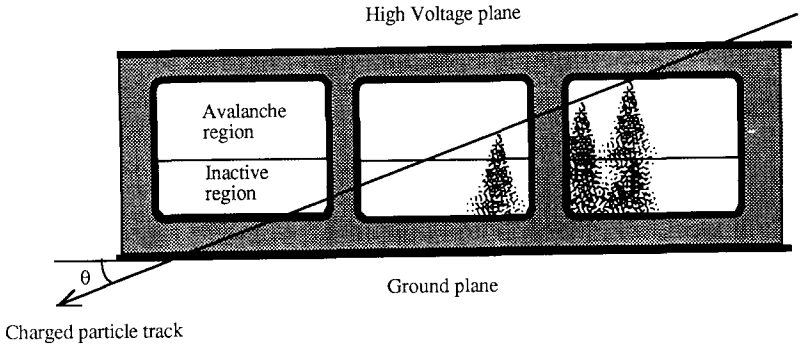

Fig. 15. Cross section of a flash chamber panel.

infers that there are on average ~ 3 available electrons per cm of gas. This is small compared to the nominal primary ionization in the neon–helium mixture which yields ~ 10 ion pairs per cm. As already mentioned, this is due to several phenomena: diffusion and attachment during the hv delay, the clearing field produced during the hv rise time, and the fact that a minimum length is necessary to initiate an avalanche so that there is an effective dead zone in each cell (fig. 15).

The amplitude and the delay of the hv pulse being fixed, the other main parameter is the gas purity. The efficiency does not vary appreciably for a large range of oxygen and nitrogen contaminations. However, the contamination is critical for achieving a rapid recombination of the plasma after the chambers have been triggered. This recombination is very slow in pure neon–helium gas and results in a sizeable reignition probability of the cells hit in the previous event. However, with standard gas conditions (~ 300 ppm oxygen, ~ 100 ppm nitrogen, gas flow: ~ 0.8 detector volume per hour), the reignition probability is 8% after 7 s and only 2% after 1 min, which is the average time between two consecutive events.

The gas contamination is also critical for the number of noisy cells which increase as the gas becomes less contaminated. The noisy cells appear preferably in the region of the hv connections where high electric fields exist. Before being installed in the detector, each FC element received about 20000 hv pulses on the test bench. This treatment reduced the number of noisy cells considerably. At present, after three years of operation and with standard gas conditions, the total number of noisy cells is ~ 250 out of a total of ~ 10^6.

During the analysis, both noisy cells and reignition are easily recognized and removed by comparing with previous events. The radioactivity contributes very little to the flash chamber noise. Measurements and estimates both indicate a contribution of ~ 10 cells.

2.3. Geiger tubes

2.3.1. Mechanics and construction of the Geiger tubes

To ensure low cost production of the required ~ 40000 6 m long Geiger tubes, these tubes are made of extruded aluminium in eight-tube units (octotubes). The cross section of this unit is shown in fig. 19a. After an internal surface treatment, each tube is equipped with a

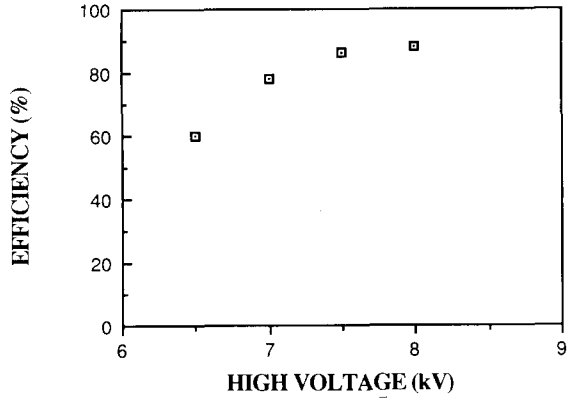

Fig. 16. Flash chamber efficiency as a function of the hv amplitude.

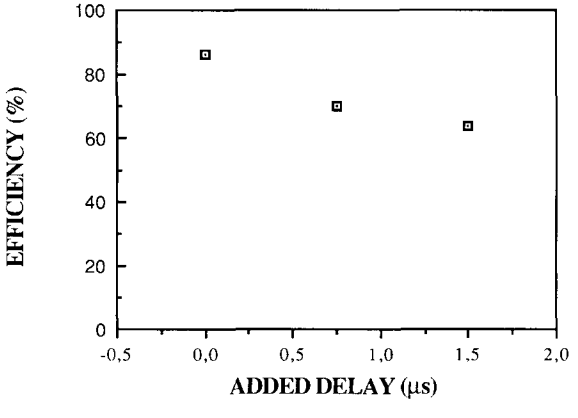

Fig. 17. Flash chamber efficiency as a function of the hv delay.

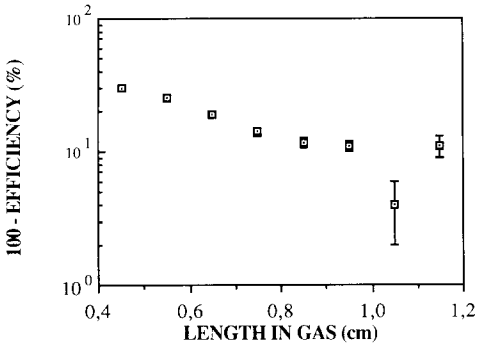

Fig. 18. Flash chamber efficiency as a function of the length travelled in the gas.

central wire by a semiautomatic threading machine [19]. The silver-coated beryllium–copper wire is 100 μm in diameter. Two spacers are placed in each 6 m tube to reduce the sagitta for a 2 m section to less than 0.3 mm. Molded plastic end plugs receive hollow copper needles through which the wire is threaded. The needles are crimped to hold the wire under a 250 g tension (fig. 19b).

Octotubes are paired forming bi-octotubes and fitted with a connector mating with the 16-channel electronic readout board (section 2.3.4.). Trigger planes are built by assembling 22 bi-octotubes on a steel structure (fig. 20). Each trigger plane (6 m $\times$ 6 m $\times$ 1.75 cm) thus consists of 352 electrically independent Geiger tubes. Trigger planes having vertical or horizontal tubes alternate, the distance between two consecutive Geiger planes being ~ 11 cm (1.45 radiation length). For the complete 900 t detector, 113 trigger planes were built over a period of two years in a 700 m^2 workshop.

2.3.2. Operation of the Geiger tubes

(1) *Gas supply*. Gas tightness is ensured by a glue joint between the tube and the end plug. Holes perforated in each intertube wall of an octotube provide for serial gas flow through the 8 tubes without external connections. The first and last plugs receive gas connections from octotubes of the same plane. The system is kept under pressure (~ 0.02 bar) to avoid air penetration, and the flow rate is 0.01 volume/h. The gas mixture (argon 98%, ethyl alcohol 2%, Freon 0.07%) is nonflammable.

The threshold voltage of the Geiger mode depends on the alcohol percentage, determined by the absolute pressure (1.7 bar) and temperature (19 °C) in the gas mixing enclosure. For a gas mixture with 2% alcohol the threshold voltage is around 1330 V. All these parameters are monitored (section 5.2).

(2) *Geiger pulse*. Positive high voltage is supplied to

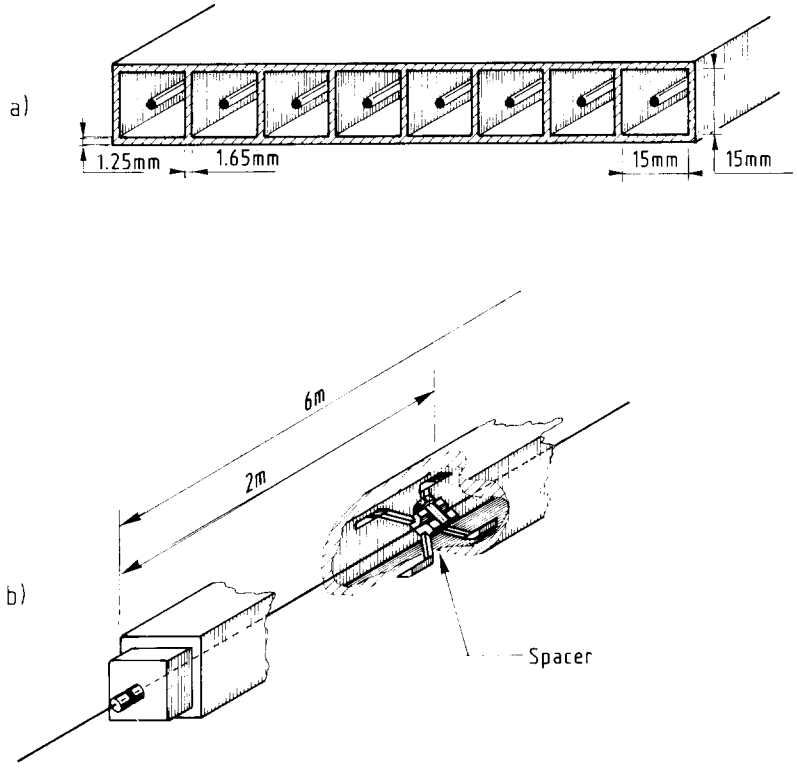

Fig. 19. (a) Cross section of a Geiger octotube. (b) Details of a Geiger tube.

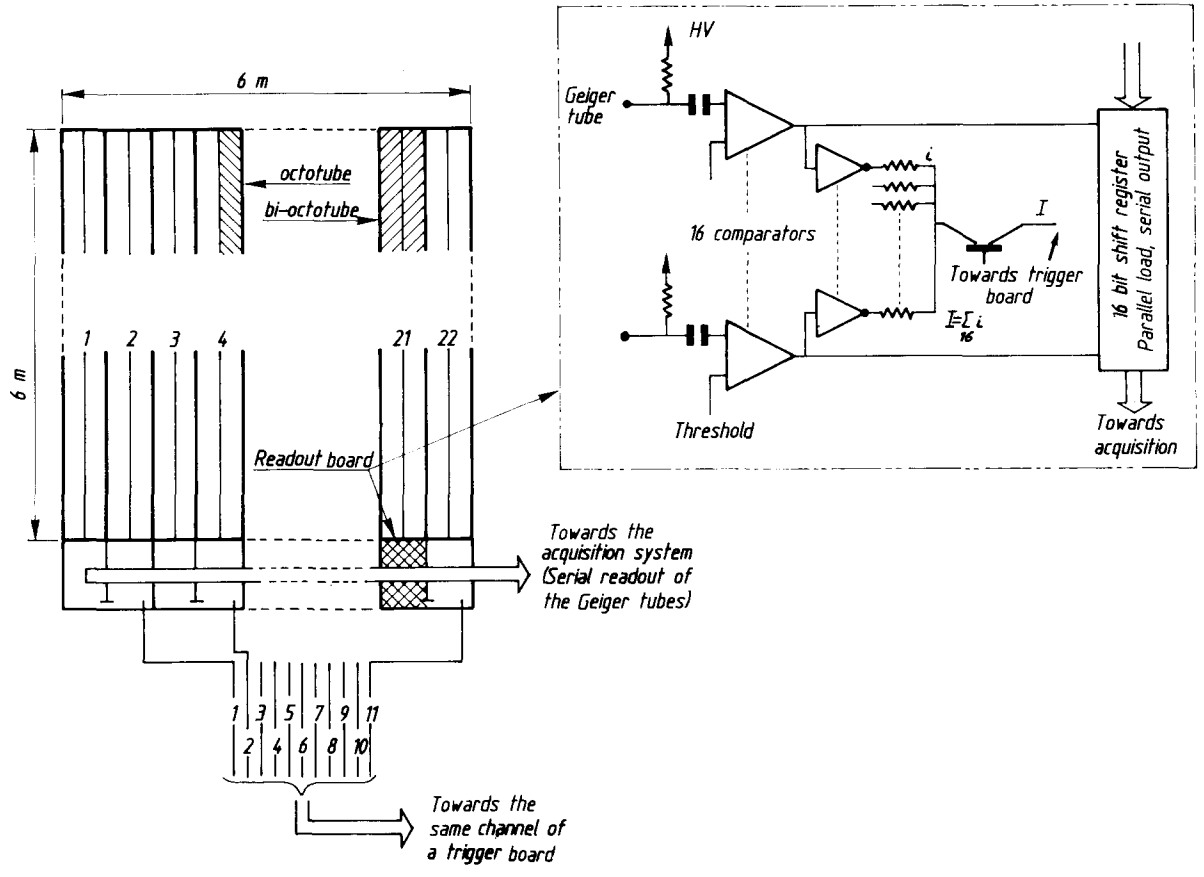

Fig. 20. Geiger plane equipped with its 22 readout boards.

the wire through the electronic readout board (section 2.3.4) which receives the Geiger pulse obtained on the wire through a coupling capacitor of 390 pF. The propagation of the discharge along the wire from the impact point of the particle stops when the end of a 2 m long section is reached. The 40–80 μs long Geiger pulse rises to about 25% of its maximum value in less than 50 ns. In the general case (fig. 21), it is a two-step pulse. The discharge propagates first in both directions along the wire providing the maximum amplitude; when the nearer spacer (or plug) is reached, the amplitude is reduced to one half. The discharge stops completely when the further spacer (or plug) is reached. The remaining signal is produced by ions receding from the wire.

Between 1350 and 1530 V the maximum Geiger pulse height increases by an order of magnitude from 25 to 250 mV on 300 Ω (the characteristic impedance of a tube).

(3) *Operating characteristics.* The counting rate of a Geiger tube in the Fréjus tunnel exhibits a plateau of about 100 V around 1480 V which is the working voltage.

The average current of a Geiger tube in a given environment is constant in the plateau region and is used together with the counting rate to monitor the Geiger tubes. In the Fréjus tunnel, it is ~ 30 μA per plane (352 tubes), corresponding to a counting rate of ~ 2400 per plane and per second (section 3.2.2.). The jitter resulting from the variable drift time of the primary electrons to the wire depends only slightly on the high voltage in the plateau region, since in this region the

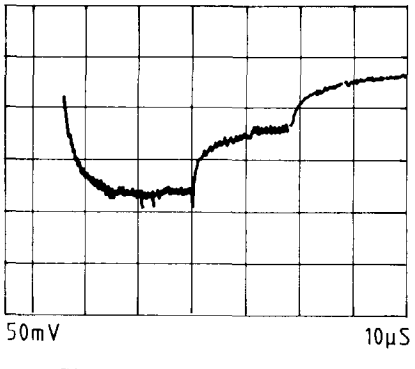

Fig. 21. Geiger tube signal pulse.

drift velocity is almost saturated. The measured value of the jitter (95% of the pulses fall within this value) decreases from 360 to 300 ns when the high voltage increases from 1350 to 1450 V. At 1480 V, more than 98% of the pulses fall within 320 ns (section 3.1.1.)

The dead time of a Geiger tube, of the order of 300 μs, is negligible due to the low counting rate.

2.3.3. Efficiency of the Geiger tubes

The first Geiger tube efficiency measurements were done with prototype octotubes using a hodoscope in an arrangement where the selected cosmic rays were practically normal to the octotube plane leading to an efficiency in the gas of about 90%. More precise results have been obtained in recent measurements using the Fréjus detector and selecting cosmic ray muons with no apparent bremsstrahlung. The efficiency, defined as the ratio $\epsilon = N_e/N_{th}$, where N_e is the number of hit tubes and N_{th} the theoretically expected number known from the reconstruction of the muon trajectory, was found to be proportional to the gas thickness crossed by the muon in the tube. However, the proportionality factor is small due to the presence of Freon (CF_3Br) in the gas mixture. The small addition of Freon is necessary to improve the pulse stability and does not drastically diminish the detection efficiency of the Geiger tubes. Since the angular distribution of cosmic muons favours vertical rather than horizontal tracks, the average Geiger tube efficiency is expected to be greater in vertical tubes (top view) than in horizontal ones (side view) as is found experimentally:

(1) vertical tubes: average efficiency 90% (average path length 18 mm);

(2) horizontal tubes: average efficiency 84% (average path length 13 mm).

Isotropically distributed charged particles due to nucleon decay or neutrino interactions would be expected to have efficiencies more like those of cosmic muons in horizontal tubes.

2.3.4. Electronic readout boards

The 16-channel electronic readout board uses the two characteristics of the Geiger pulse: steep rise to build a fast trigger, long duration as a built-in memory essential for reliable readout in an environment containing flash chambers. The input stage of each channel, consisting of a common base transistor followed by a voltage comparator, has a sufficiently low threshold (6–30 mV on 300 Ω) to provide triggering on the fast-rising part of the Geiger pulse (section 2.3.2). Each comparator has two functions. For readout it furnishes a voltage level to the parallel input of a CMOS shift register. Since this level lasts essentially as long as the Geiger pulse (40–80 μs), the load pulse can be applied well after the noise induced by the flash chambers has disappeared. At present the delay is 20 μs. The second and main function of the comparator is to contribute to the trigger. It furnishes a current signal i of standard amplitude to a 16-channel summing network on the board. To get the contribution of a plane the current signals from the 22 readout boards (fig. 20) are first added locally two by two and then sent through 11 cables (7 m long) to the same channel of a trigger board.

3. Trigger logic and performance

3.1. Trigger logic

3.1.1. Basic elements of the trigger electronics

The 23 five-channel trigger boards (fig. 22) are distributed along the detector and interconnected to constitute a continuous system with no internal boundaries. Each channel (fig. 23) consists of an 11-input summing network followed by an adjustable 280–400 ns clip line. The duration of the 40–80 μs current pulse is thus reduced to 320 ns, compatible with the jitter (section 2.3.2). The maximum signal amplitude on the clip line will be proportional to the number of time coincident pulses. This signal is presented to a limiter M consisting of four comparators used to regenerate the currents and allowing for a contribution of at most m tubes in a plane ($1 \leq m \leq 4$).

This information is then sent together with that coming from adjacent planes to a summing network P for p consecutive planes ($1 \leq p \leq 6$) followed by a comparator S requiring s tubes ($1 \leq s \leq 6$) to provide a trigger signal. This circuit configuration is repeated for each of the 109 possible associations of p consecutive planes. It is achieved in three steps using OR circuits. A first step OR circuit on the trigger board (fig. 22) mixes the output signals of the five channels. The output signals of five consecutive trigger boards are further combined in the following OR circuit. The master trigger unit mixing the output signals of the five groups of trigger boards provides the final trigger to the flash chamber high voltage system ~ 1.2 μs after event production. Note that the master trigger unit receives a flash chamber veto signal and an anticoincidence antenna signal discussed below (section 3.2.3).

3.1.2. Trigger parameters

The trigger parameters m, p and s were chosen with reference to the characteristics of nucleon decay events. The *multiplicity parameter m* controls the effect of the showering properties of electrons and photons, as well as that of pion interactions and steeply inclined tracks. The *range parameter p* applies to the physical extension of a nucleon decay event. The *threshold parameter s* characterizes the fraction of its total energy used to trigger. Increasing m and p means considering a greater

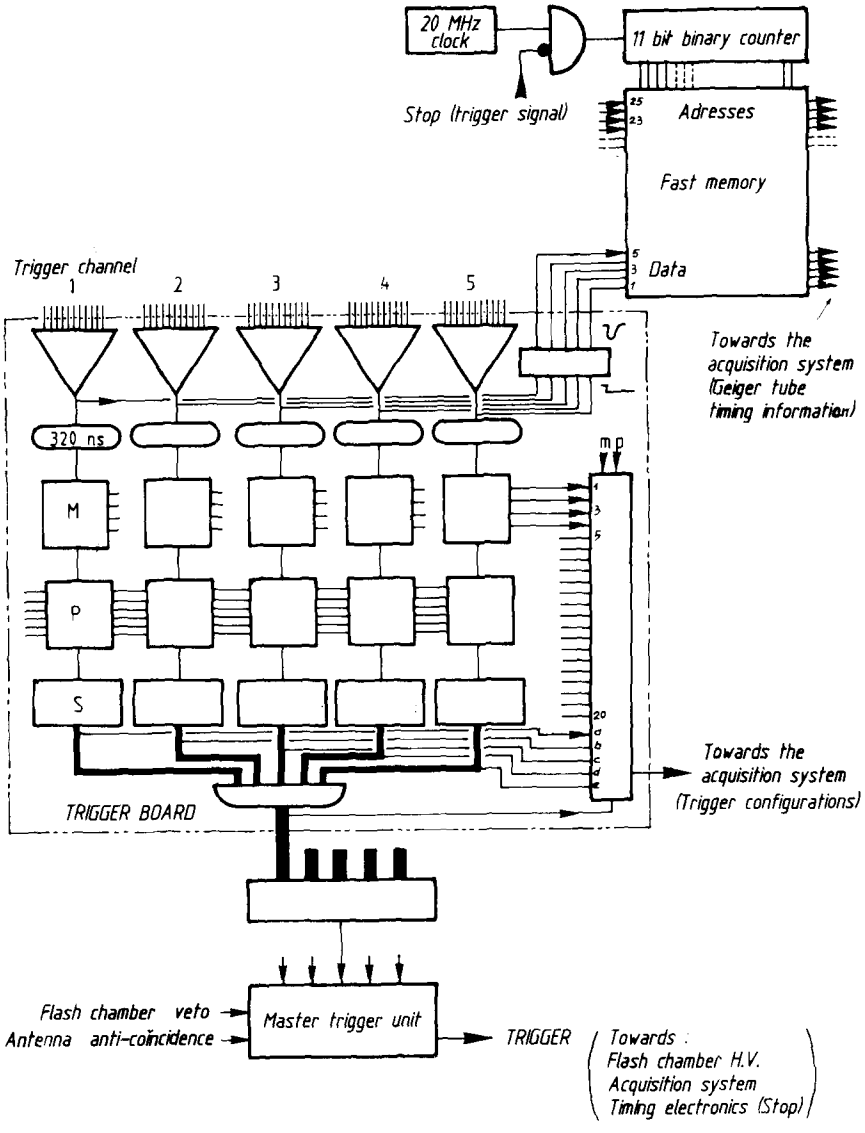

Fig. 22. General layout of the trigger board.

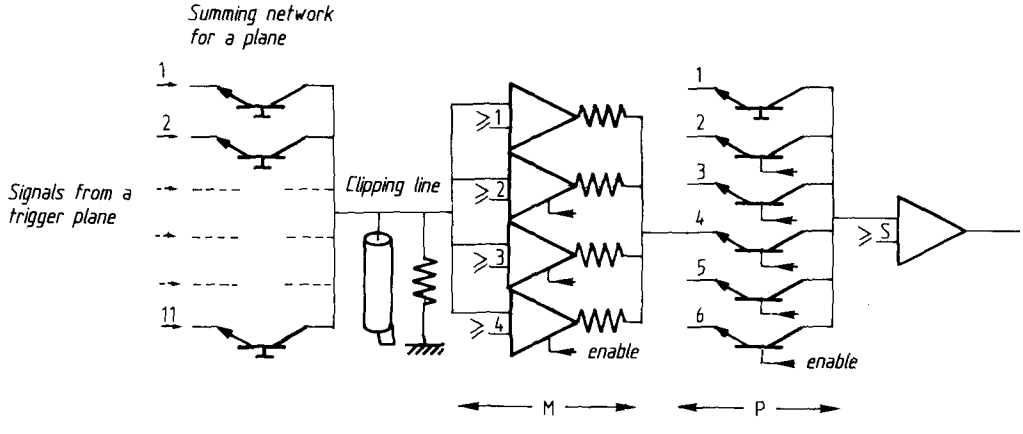

Fig. 23. Trigger channel: M = limiter allowing for a contribution of at most m tubes in a plane ($1 < m < 4$); P = summing network for p consecutive planes ($1 < p < 6$); S = comparator requiring at least s tubes ($1 < s < 6$). The binary levels on the ENABLE lines are set to provide the desired m and p values.

volume in which the nucleon decay event is examined, thereby increasing both trigger efficiency and background trigger rate. Lowering s means a smaller number of tubes, equivalent to a lower coincidence level required to provide a trigger, thus again increasing both trigger efficiency and trigger rate. The variation limits of the trigger parameters were one of the main concerns when defining the trigger electronics. Those chosen have proven wide enough to define a set of values under working conditions which provide low background trigger rate and high trigger efficiency: $m = 3$, $p = 5$, $s = 5$.

Thus a trigger will be produced if at least five Geiger tubes have fired within 320 ns in at least one association of five consecutive planes, each plane contributing with 0, 1, 2 or at most 3 tubes.

3.1.3. Trigger configurations

Reading out the Geiger tubes for each trigger does not generally provide sufficient information on the combination (or combinations) of tubes actually responsible for the trigger. Such information is important for trigger consistency tests, monitoring purposes and particle signature. A shift register on each trigger board (fig. 22) is connected to the static trigger parameters m and p, used here as fiducial marks, to the four comparator outputs of each of the five limiters M (inputs 1, 2, 3, 4, $\cdots$, 20 on the shift register) and to each of the five trigger channel outputs (inputs a, b, c, d, e on the shift register). A load signal produced by the earliest triggering combination thus stores on all boards the instantaneous state of:

(1) the trigger parameters m and p,
(2) the lines giving the contribution to the trigger of each plane (0, 1, 2 or at most m tubes),
(3) the output signals showing the location of the triggering combination(s) which have contributed.

It should be emphasized that the trigger configurations do not provide all the triggering combinations which occur within the 320 ns resolution time, but only the earliest ones. To be of any use, the stored information must survive the duration of the flash chamber pulse.

3.1.4. Timing information

The timing information electronics is part of a system built to detect magnetic monopoles using the Geiger tubes of the Fréjus detector. This is possible since the Geiger tube signal lasts long enough to follow a slow moving magnetic monopole ($\beta = 10^{-3}$ to 10^{-1}) through as many as 25 Geiger planes. The complete monopole detection system, which requires a special trigger, will be described in a separate paper. Only the timing information electronics used independently in both the monopole and proton decay experiments will be described here. Geiger tube timing information is provided by a continuously cycling 20 MHz memory 113 bits wide (one per plane) and 2048 bits deep. The system consists physically of five 25-channel modules (fig. 22). A sample is stored every 50 ns indicating for each plane whether or not a new Geiger tube signal arrived during that period. The cycling is stopped by the trigger just before the arrival of the flash-chamber noise, typically about 1 μs after the first Geiger signal from the event. The data stored provides the "history" of an event: the time of arrival of the pulses in each plane during the 100 μs preceding the memory stop pulse. In spite of its limitations (no information for Geiger pulses arriving during or after the flash tube pulse, no space–time correlation in case of more than one hit per plane, minimum pulse separation 50 ns), the timing information is useful for monitoring purposes and spurious hit elimination.

3.2. Trigger rate and trigger efficiency

3.2.1. Muon rate

The necessity of having a low trigger rate is inherent to the nature of the detector: the flash chamber dead time which is set to 4 s and the limited life time of the spark gaps. Clearly, in the absence of an active veto shield, the lower limit of the trigger rate is given by the cosmic muon rate which is reduced in the Fréjus tunnel by a factor $\sim 10^6$ with respect to the rate at the surface of the earth. It has been measured during the installation of the detector to vary, as expected, linearly with the size of the detector:

$$\text{muons/h} = 0.15N + 2.5, \qquad (2)$$

where N is the number of trigger planes. For the complete detector ($N = 113$) the muon rate is about 20 muons/h.

3.2.2. Accidental trigger rate

The accidental trigger rate is due to radioactivity which is responsible not only for the singles, but also for time correlated twofold and threefold real coincidences in the same Geiger plane: the singles rate per plane and per second is 2400 ± 200, the twofold rate 23 ± 2, and the threefold rate 0.21 ± 0.03.

Three main radioactive sources contribute:

(1) γ-radiation from the surroundings: rock, concrete and air (radon),
(2) γ-radiation due to ^{60}Co contamination of the detector's iron plates,
(3) β-radiation due to ^{238}U contamination of the aluminium Geiger tubes [20].

After calculating accidentals for various sets of trigger parameters, especially for those involving only fourfold coincidences ($s = 4$) which would lead to higher efficiencies, one is forced to conclude that the set of values finally chosen (section 3.1.2) is the only accepta-

ble one. The calculation has to take into account all the combinations of chance coincidences within 320 ns between five Geiger tube pulses in an association of five consecutive planes, each plane contributing with 0, 1, 2 or at most 3 pulses. The main contributions come from threefold–double, single–double–double and threefold–single–single chance coincidences. The calculation also has to take into account the measured average coincidence time of 50 ns for the real double coincidences and 110 ns for the threefold real coincidences in the same plane and should not neglect double coincidences between two consecutive planes (1.8 counts/s) and double coincidences between two planes separated by a third (0.7 counts/s). The calculated accidental trigger rate as a function of the number N of Geiger planes is:

$$\text{accidentals/h} = (0.135 \pm 0.025)N. \quad (3)$$

This relation is in excellent agreement with the experimentally measured background rate when the flash chamber system is not operating (no electromagnetic noise) and leads to a lower limit of the background for the complete detector ($N = 113$) of (15 ± 3) counts/h. A higher trigger rate due to accidentals occurs very rarely and is usually the result of overshoot or drift in the amplitude of the time coincident signals leading locally to a trigger equivalent to $s = 4$. The diagnosis of such a situation using a forbidden configuration test is extremely easy (section 5.2) and the normal situation is rapidly restored. A decrease in the accidental trigger rate, on the other hand, is extremely dangerous since it could, locally at least, correspond to an $s = 6$ trigger which would drastically reduce the trigger efficiency.

For this reason, the accidentals rate distribution is monitored on-line allowing to localize the trigger board responsible for such a situation (section 5.2).

3.2.3. Trigger rate due to electromagnetic noise and the antenna anticoincidence system

The noise trigger rate is essentially due to electromagnetic noise pickup and occasionally to arcing in the Geiger high voltage system. The output signals are short and not recorded by the readout.

Although a 4 s veto signal prevents retriggering until the flash tube system is ready to fire again, the electromagnetic noise remains high for several more seconds and is capable of triggering the Geiger tube electronics, thus producing a prohibitive noise rate (up to an order of magnitude higher than the accidentals rate). Local shielding of the Geiger tube readout boards was not sufficient. A solution was found using a set of 16 antennas distributed all along the detector in the neighborhood of the pulsers. Each antenna is connected to an adjustable-threshold discriminator sensitive to signals in the 5 mV range. The output pulses go into an OR circuit and the result is sent to a 10 μs anticoincidence circuit in the master trigger unit (fig. 22). The average counting rate of an antenna (section 5.2) is in the range of 1 to 100 counts/s. Thus the dead time induced is practically negligible ($< 1\%$). The antenna anticoincidence system keeps the noise trigger rate under working conditions within narrow limits of 5 to 15 counts/h. This somewhat variable noise trigger rate is inherent to the dynamic, day to day, situation of the detector: a pulser may become particularly noisy, an antenna discriminator may need readjustment, and, as already mentioned, high-voltage arcing in the Geiger system may cause trouble. In any case, the noise trigger rate is not allowed to contribute much more than the accidental rate, so that the typical background rate (accidentals = noise) is $\sim (25 \pm 5)$ counts/h. The on-line monitoring information (section 5.2) is usually sufficient to locate the source of an excessive trigger rate.

3.2.4. Total trigger rate and dead time

The total trigger rate (muon rate + background rate) of about 45 h^{-1} is reasonable from the point of view of pulser life time and introduces a dead time loss through the 4 s veto time of only $\sim 5\%$.

3.2.5. Trigger efficiencies for various processes

Nucleon decay modes without neutrinos for which all the energy (~ 1 GeV) is left in the detector have been generated by Monte Carlo calculations. The trigger efficiency has been studied as a function of the trigger parameters m, p and s and the average Geiger tube efficiency ϵ_G. For $m = 3$, $p = 5$ and $s = 5$ and for $\epsilon_G = 90\%$, the trigger efficiencies are high for all typical modes such as $p \to e^+\pi^0$, $p \to \mu^+K^0 \to \pi^+\pi^-$, $n \to e^+\pi^-$, $p \to e^+\rho^0$, $p \to \mu^+K^0 \to \pi^0\pi^0$. We find that the trigger efficiency ranges from 80% to 90%. These efficiencies decrease by only about 3% when the Geiger tube efficiency is reduced by 5%.

For modes with a neutral lepton such as $p \to \bar{\nu}K^+$, $p \to \bar{\nu}\rho^+$, $n \to \bar{\nu}\pi^0$, $n \to \bar{\nu}\eta^0$, $n \to \bar{\nu}K^0$ the trigger efficiencies lie between 10% and 60%.

The trigger threshold for low energy single muons is 200 MeV/c and the trigger efficiency reaches 50% at 350 meV/c. This result has been obtained independently in two ways: experimentally by analyzing stopping muon tracks, and by Monte Carlo solution using a 84% Geiger tube efficiency. The same Monte Carlo study for low energy single electrons shows a threshold at 150 MeV/c and a trigger efficiency reaching 50% at 420 MeV/c.

4. Data acquisition

4.1. Basic requirements for data acquisition and on-line monitoring

The data acquisition and monitoring was designed

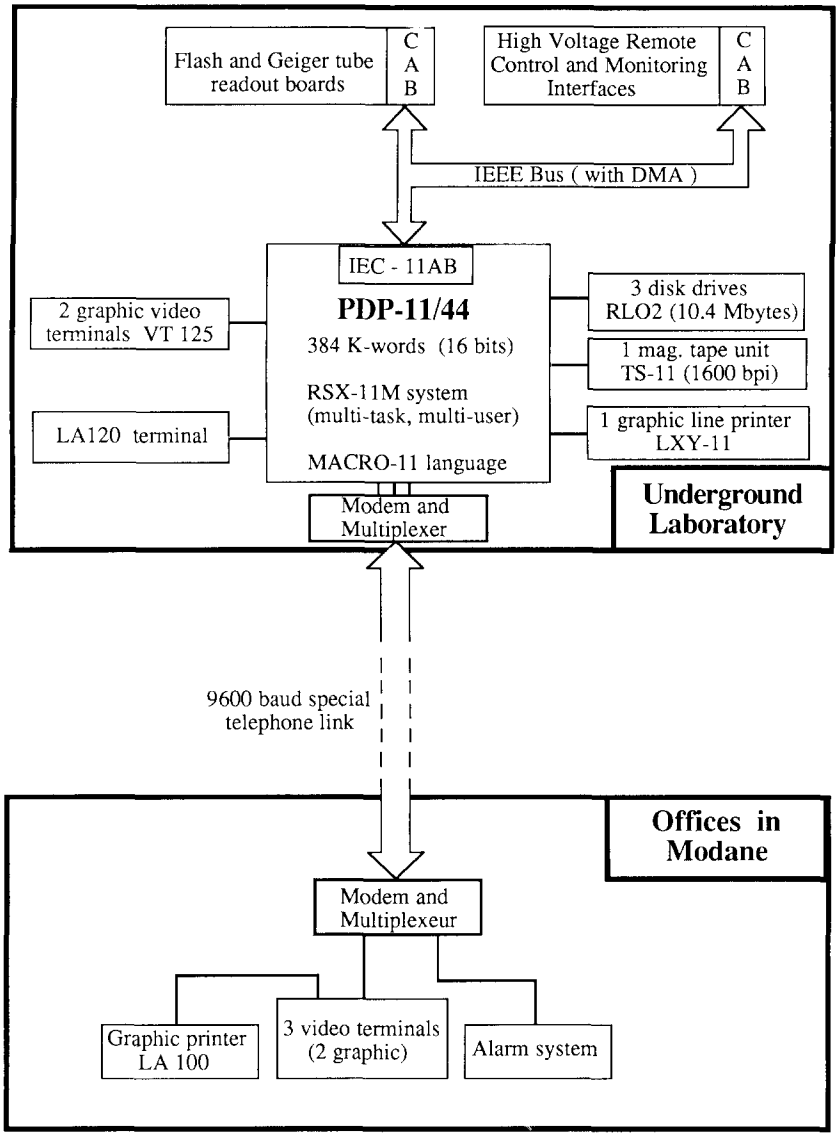

Fig. 24. Data acquisition system: hardware layout.

on the basis of the following requirements:

(a) A typical event (single cosmic ray muon) consists of about 800 fired flash tubes, out of a total of 0.93×10^6 tubes. Some rare events have as many as ~ 50000 hit tubes. In order to collect the addresses of the hit channels as quickly as possible, a fast microprocessor (200 ns cycle time) acting as a crate controller is used together with eight CAMAC boards. This fast processor is referred to as "CAMAC booster" or CAB [21]. It also reads out the addresses of the hit Geiger tubes, as well as the trigger configurations. Self-consistency checks are continuously performed by the CAB during the readout sequences and anomalous situations (e.g. wrong fiducial marks) are recorded. Two CABs, each controlling one CAMAC crate, are used in the experiment: the first one is essentially concerned with flash tube and Geiger tube readout; the second is devoted to various monitoring tasks. Both processors are linked to the main computer, a PDP 11/44, through an IEEE bus [22] as indicated in fig. 24.

(b) A nucleon decay experiment must be operated continuously for several years in an isolated site. Therefore, a remote control providing automatic diagnostics and alarms is required. The PDP 11/44 is located in the underground laboratory, together with disk and magnetic tape units (fig. 24). However, the experiment can

be controlled from offices in the nearby town of Modane by using several VT 125 graphic terminals and an alarm device, connected to the main computer by means of a specialized link (9600 b rate). Physicist's intervention in the underground laboratory is only required in the case of severe alarms (e.g. power failure, safety alarms, high currents in pulsers, anomalous trigger rates).

(c) Running conditions must be recorded on specialized disk files, which can be modified by using editing routines.

(d) Data are continuously stored on an RL02 disk. Its capacity of 10.4 Mbytes corresponds to about 1.5 d of data taking. Every day, events are copied onto magnetic tapes. Of course, this operation does not stop data taking.

(3) Independently of diagnoses and alarms, the experiment is further monitored through a first analysis of the data:

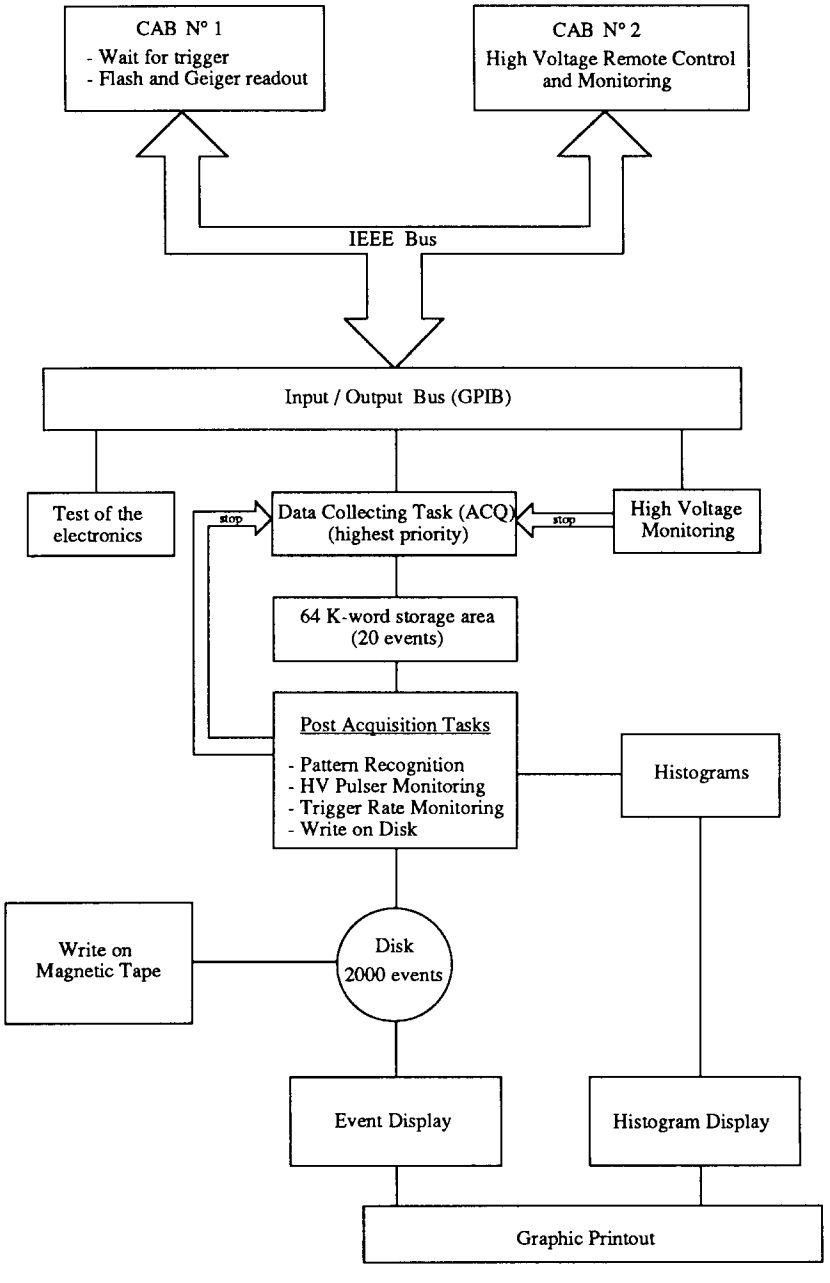

Fig. 25. Data acquisition system: software layout.

(1) an event display facility allows the physicist to classify and tag events as soon as they occur;
(2) flash and Geiger tube efficiencies are calculated from single muon events;
(3) noisy tubes are recorded; flash tube elements with a poor efficiency can be found within a few days of data taking;
(4) various histograms can be displayed on operator request.

(f) Hardware as well as software developments should be compatible with data taking. The multitask and multiuser system RSX-11M is used on the PDP 11/44. Access to the CABs, i.e., to the CAMAC crates, can be provided for any task during the dead time of the detector, thus allowing tests of the hardware on request.

4.2. General software layout

The general software layout is indicated in fig. 25. In the acquisition of an event, we distinguish the three following steps:

(a) Fast processing takes place in the CAB microprocessors. The CAB concerned with flash (or Geiger) tube readout sends the addresses of hit tubes (ordered in longitudinal rows) to the PDP 11/44.

(b) In the PDP 11/44, a high priority task (the highest priority task after the executive), referred to as ACQ, requires data storage through DMA (direct memory access) into a dedicated area of the memory of 64K words, equivalent to about 20 events, i.e. about half an hour of data taking. This allows ACQ to reactivate the CAB program, which will then wait for a new trigger, without caring about further event processing and writing on disk.

(c) These further tasks are handled by programs with a priority level just one step below that of ACQ. They will be referred to as post-acquisition tasks.

Besides the acquisition operations, the following facilities are provided:
(1) event display and printing,
(2) histogram storage, display and printing,
(3) editors (cabling configurations, monitoring parameters for high voltage and currents),
(4) procedure to copy events from disk to tapes.

The data transfer between the CABs and the PDP 11/44 through the IEEE bus is handled by the IEC-11A/B interface provided by Digital Equipment, and the corresponding "driver" routine. However, this driver can only be used by one task at a time. In order to permit access to the CAMAC crates from different tasks, a general utility, named GPIB, has been written in order to handle their requests and to transmit them to the driver. GPIB also provides automatic CAB loading with the program selected by the user. Easy access to GPIB for bus commands or data transfers is provided by a library of MACRO instructions. Finally, facilities for CAB programming (assembler, loader, debugger, $\cdots$) are available.

All the preceding programs have been written in assembler language (MACRO-11 for PDP 11/44 tasks).

4.3. Event recording

As soon as an event has been stored in the memory of the PDP 11/44, the ACQ program waits for the enable from the flash chamber hv, re-enables the triggering electronics and records the time at which the detector is again active. The CAB responsible for flash and Geiger tube readout is re-activated. Once a trigger signal is received by the CAB, the PDP 11/44 is interrupted and ACQ records the trigger time; this allows a complete book keeping of the life time of the detector. When ACQ is stopped on operator request, a dummy event is generated, in order to record the time of the stop.

Since January 1987, Universal Time has been measured with an accuracy of 1 ms by means of a local oscillator which is regularly calibrated by signals from radio station France-Inter.

The fast processing in the CAB is then started; each CAB sequence corresponds to a given set of tubes (flash or Geiger) and to a given view (top or side). Each CAMAC board devoted to flash and Geiger tube readout includes 64 input lines, each one corresponding to the serial output line of a plane from a given view; the latter is selected by setting a particular multiplexer address, as indicated above. One CAMAC board handles 8 supermodules; 8 boards are necessary for the flash chamber acquisition; one additional board is devoted to Geiger tubes.

Within a single CAMAC cycle, the CAB sends the clock signal to all planes; the bits appearing on the input lines are then latched into 16-bit registers in the CAMAC boards; they represent the contents of a longitudinal row of tubes, i.e. of tubes with a fixed transverse coordinate (X or Y). If no such tube in the row is hit, no "look-at-me" signal (LAM) is emitted by any CAMAC board, and the CAB sends another clock signal in the next CAMAC cycle, which corresponds to the next value of the transverse coordinate (X or Y). If at least one hit is detected, the CAB can easily determine the addresses of fired tubes by means of priority encoders. Since the CAB can execute five instructions per CAMAC cycle, this logic allows to minimize the readout time. All readout incidents (anomalous "busy" signal or wrong fiducial marks) are recorded. A typical event, e.g. a single muon with 800 fired tubes, requires about 20 ms of CAB time and 30 ms of transfer time on the IEEE bus.

When the preceding data have been collected, ACQ takes control of the second CAB (whereas the first CAB

is left free for other users during the dead time of the detector). Data from the pulser monitoring system are then read out by the second CAB and the value of the flash chamber high voltage is checked and corrected if necessary. The acquisition of the event is completed when all monitoring data have been stored into the PDP 11/44.

Events are further copied onto the disk by means of a postacquisition task. Prior to this operation, a simple pattern recognition analysis (including the tagging of noisy cells and cells due to reignition) is performed, to be used for further monitoring of detector efficiencies. Each event is written on a separate file on disk; this allows several users to access events at the same time for display or additional calculations. The postacquisition task also creates a special directory in which addresses of events on the disk are recorded in chronological order. In such a way, a long search in the system directory can be avoided when events are copied from disk to tapes; data from one full day of running are copied twice in about 20 min.

5. Detector monitoring

5.1. General description

The monitoring of the detector was designed with three objectives in mind. First, the detector performance is checked continuously to make sure that tracks are recorded efficiently and that the trigger rate is kept within normal limits. Second, because the detector is remotely controlled from outside the laboratory, it is necessary to be able to "shut down" the detector in case a potentially dangerous anomaly is detected. Finally, the monitoring provides means for easy maintenance by localizing defective hardware (e.g. high voltage pulsers which need replacing, Geiger tubes responsible for high trigger rates) and for detecting possible long term variations of detector properties.

During data taking, the events on disk are used for monitoring the detector's performance. All events are systematically examined on one of the graphic video terminals. Using muons, the detection efficiency of

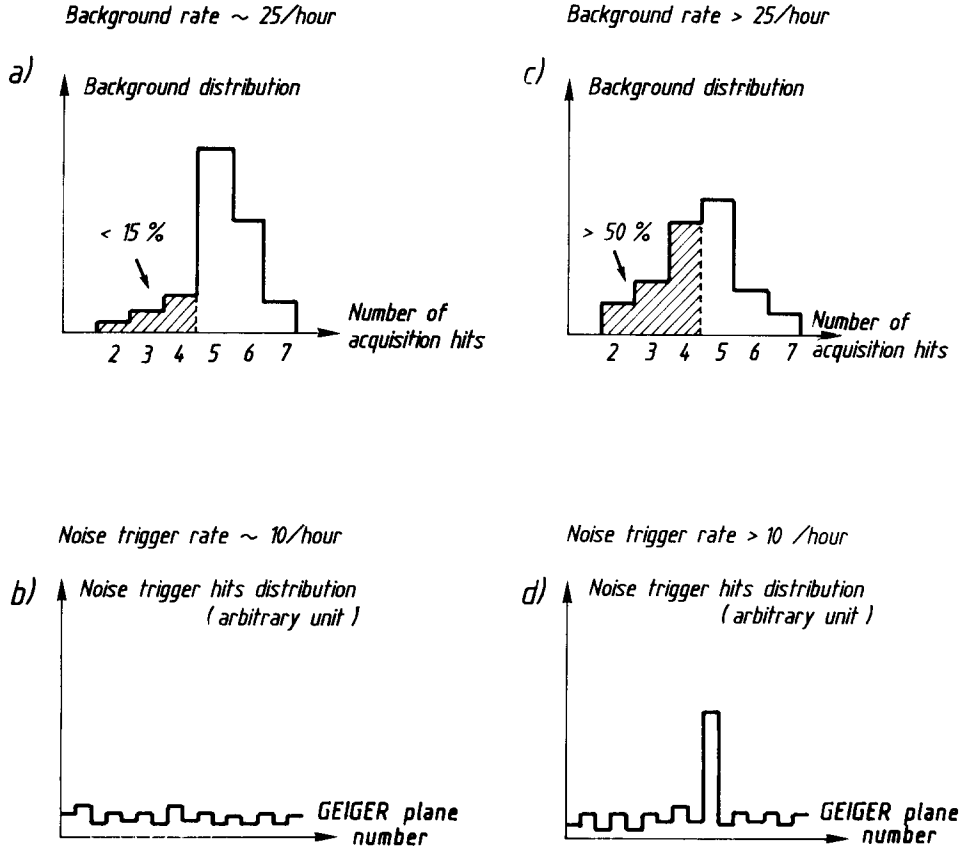

Fig. 26. Typical normal (a, b) and abnormal (c, d) trigger behaviour.

Geiger planes and flash chambers as well as the number of noisy cells in the detector are determined and provide a global monitor of the quality of the recorded data. In particular, with muons recorded over periods of several days, the efficiency and the reignition probability of each flash chamber plane can be obtained and serve as a guide to adjust the individual thresholds for the flash chamber pickup signals.

5.2. *Monitoring of the Geiger tubes*

On-line monitoring uses test programs running during the 4 s dead time interval after each trigger, and analysis programs which produce, Geiger tube hit distributions, timing information (section 3.1.4) and trigger configuration (section 3.1.3) histograms for recently recorded events. Some of these programs require prior on-line scanning by the physicist on shift who classifies events as energetic particles (mainly muons) or background. Others compare the trigger configuration information with the tubes seen on readout in order to separate the two components of the background. Accidentals (section 3.2.2) have a configuration equal to the trigger threshold ($s = 5$) and correspond to five or more tubes hit. Noise triggers (section 3.2.3) provide a valid trigger configuration but the corresponding readout hits are partially or totally absent. The following quantities characterize the trigger system and are monitored during data taking:

(1) The muon and background rates.
(2) The trigger rate due to accidentals.
(3) The average efficiencies for vertical and horizontal Geiger tubes.
(4) The readout hits of each tube of a plane (this relatively long measurement is normally done off-line).
(5) The singles counting rate of each plane.
(6) The antenna counting rates.
(7) The Geiger gas constants.
(8) The number of readout hits in the triggering association of five consecutive planes for each background event. The distribution of this value has a maximum for 5 hits, a $\leq$ 4-hit contribution of $\leq 15\%$ when the background is normal (fig. 26a) and a much greater contribution ($\gg 15\%$) if it is abnormal (fig. 26c).

Any discrepancy from the expected values has to be rapidly understood and corrected. To do this, additional information is available from the following histograms providing information on:

(1) High voltage and current of each plane.
(2) The readout hit contribution from each plane.

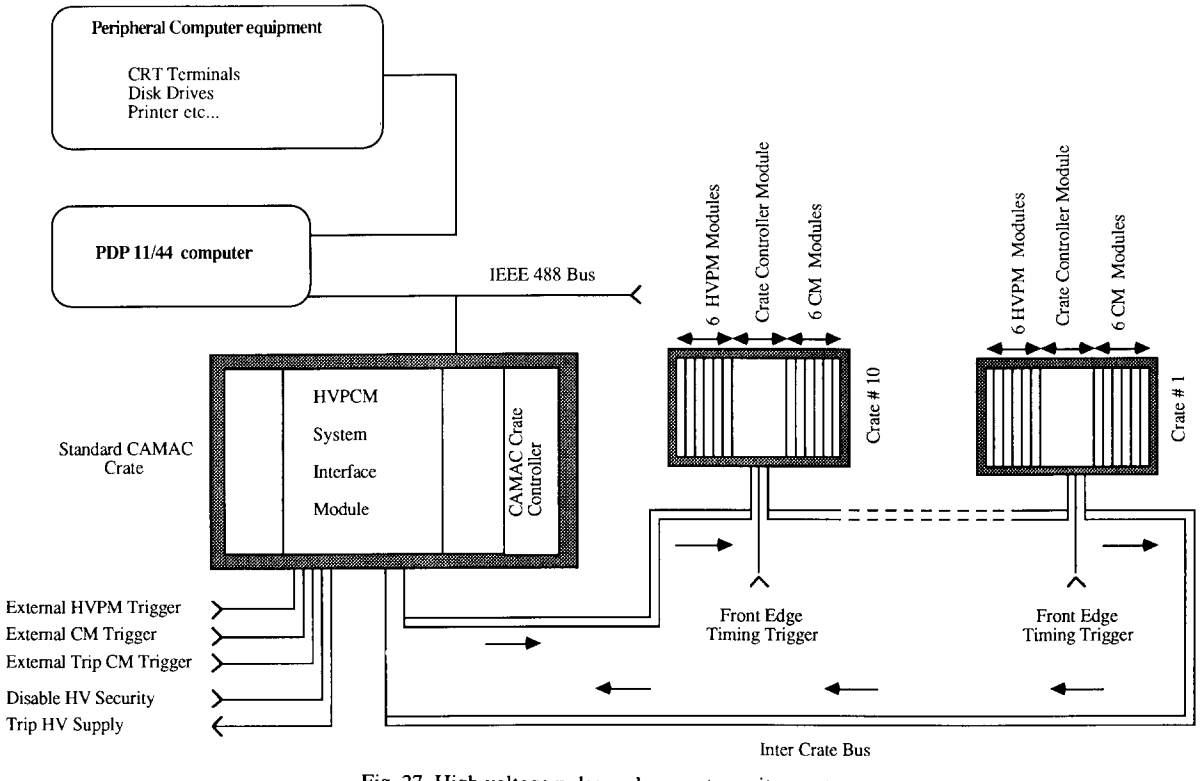

Fig. 27. High voltage pulse and current monitor system.

(3) The singles rate contribution to the trigger from each plane.
(4) The muon trigger hit contribution from each plane.
(5) The single, double and triple hit contributions from each plane for accidental triggers.
(6) The noise trigger hit contribution for each plane (fig. 26b, d).

Thus any missing plane or any significant deviation from a flat distribution can be localized. The main cause for trigger instabilities come from the noise trigger rate. A typical normal (a, b) and abnormal (c, d) trigger situation is shown in fig. 26. Histogram (d), by localizing the problem, is particularly useful for re-establishing the normal trigger situation.

Off-line monitoring completes the supervision of the Geiger system. By reading out each Geiger plane with and without a trigger, it is possible to verify that all tubes are read and participate uniformly. The singles, twofold and threefold coincidence rates of each plane are checked periodically using scalers. No contribution to the accidentals at the $s = 4$ level is tolerated. This is checked using test signals which simulate the contribution to the trigger of 1 tube in each plane. No trigger should occur when the trigger parameters are set to the forbidden configuration $s = 5$, $p = 4$, $m = 1$. The antenna behavior and counting rates, responsible for efficient anticoincidence of electromagnetic noise, is checked. Finally the Geiger gas system parameters are checked: flow, pressure and temperature, alcohol and Freon percentages.

5.3. Flash chamber monitoring

Together with the FC gas contamination measured with the gas chromatograph, the efficiency and reignition measurements using muons provide a monitor of

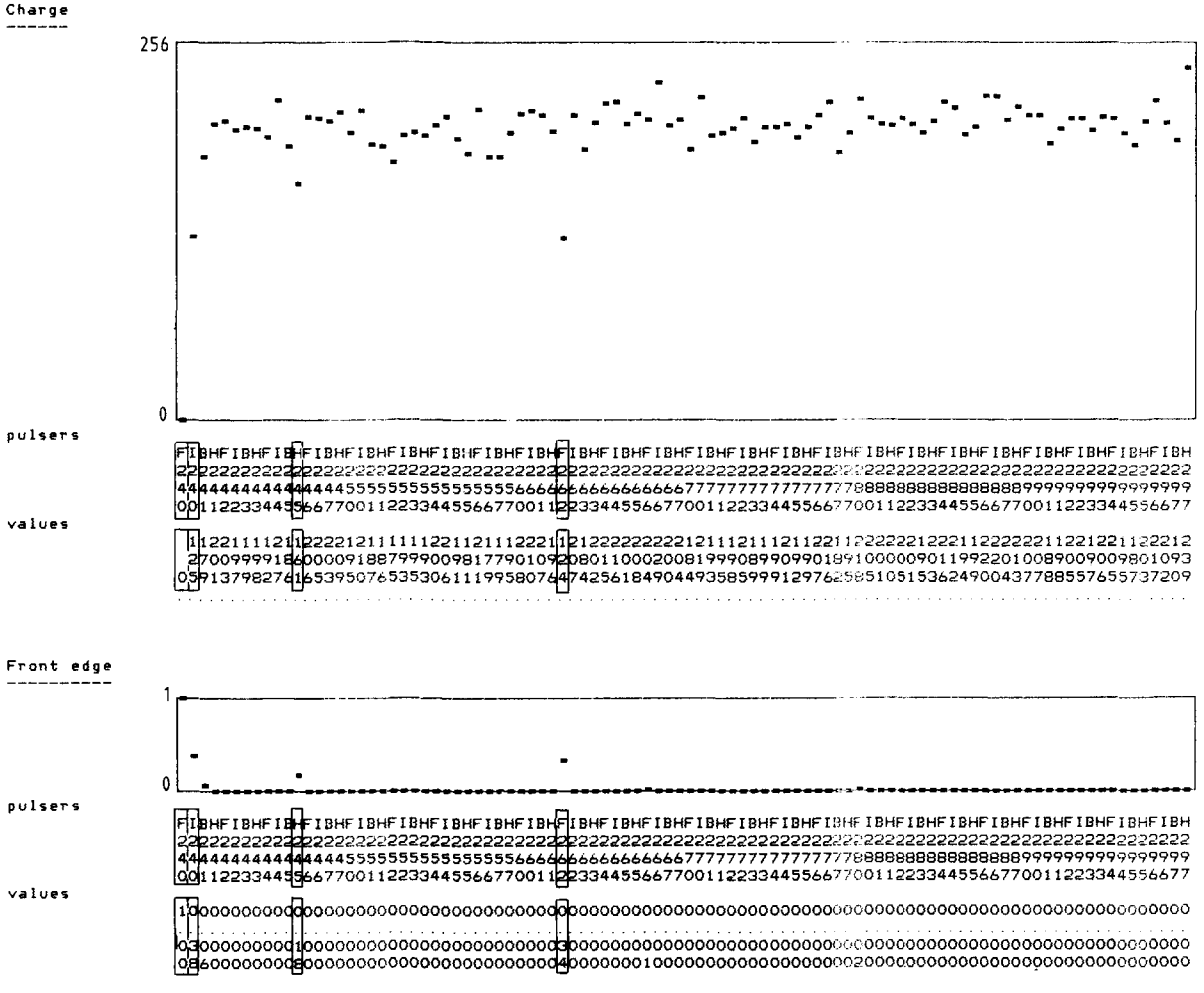

Fig. 28. High voltage pulse and current monitor data.

the quality of the gas and determine whether switching to a new purification column is needed.

Because of the large number of elements in the hv system, it was necessary to build a computer controlled monitoring system. The high voltage pulse and current monitor system (HVPCM) is used to check if a proper hv pulse is applied to each flash chamber at every trigger and to detect the failures of the pulsers or other hv equipment. Insulation defects which appear between flash chamber electrodes and short circuits of the storage hv delay lines occur occasionally. The most common failures are misfiring spark gaps. These devices deteriorate with time because the enormous currents which are flowing produce mechanical and chemical damage to their electrodes.

Except for a few modifications, the HVPCM is similar to the system described in ref. [23]. It monitors the 912 hv channels and consists of ten crates of electronics distributed along the detector. It is interfaced to the computer via a CAMAC module controlled by one of the CABs. A block diagram of the HVPCM is shown in fig. 27. At each trigger the HVPCM measures the total charge in each of the 912 hv pulses applied to the flash chambers, checks if the pulse is applied at the proper time, and verifies if there is spurious sparking between triggers. The system also measures the recharging current of the 912 hv channels at a fixed time after a trigger.

Analysis of the HVPCM data makes it possible to detect most failure modes of the hv system. For example, the data in fig. 28, which are available on-line, shows that the average total charges of pulsers F240, I240, H245, and F262 are too low and are due to, respectively, 100%, 38%, 18%, and 34% of missed pulses. This information is used to guide the maintenance work on the spark gaps.

The hv current monitor has a feature which makes it possible to automatically turn off the hv when any of the pulsers has a recharging current above a preset threshold (100 μA, 3.3 s after the trigger).

Besides being a guide for maintenance, the HVPCM, and in particular the current monitor, makes it possible to safely run the experiment from outside the laboratory.

5.4. Remote control of the experiment

The experiment is being run most of the time from offices in Modane via telephone links to the data acquisition computer and the laboratory surveillance automaton. At least once a day, a visit is made to the laboratory to go through a safety oriented check list and copy events from disk to tape.

Monitoring software has been developed to use the HVPCM not only as a help for maintenance but also to detect potentially dangerous failures such as repeated overcurrent in a hv channel. In such an event, the alarm procedure is activated: hv is turned off automatically, data taking is stopped and a warning message is sent to all terminals and over the radio system to alert the physicist on call for immediate intervention. In most cases the HVPCM gives a precise diagnosis for the incident. Other crucial parameters which are monitored include the status of the gas purification system, the nitrogen pressure in the spark gaps, the trigger rate and the space available for events on disk. If any one of these is abnormal or if one of the safety parameters from the laboratory itself (such as fire alarms, lack of air conditioning in the computer room) is abnormal, the alarm procedure is also activated.

5.5. Maintenance and long term behavior of the detector

The full 900 t detector has been operating since June 1985. The most important maintenance effort goes into the flash chamber hv pulsers. Occasional trigger rate variations also make interventions on the Geiger tubes necessary. The average fraction of time during which the experiment was taking data is 80%.

5.5.1. Geiger tubes

After three years of operation the fraction of Geiger tubes out of order is less than 1.5%. There are 57 broken wires, 128 very noisy wires and 25 bi-octotubes are disconnected because of a prohibitive sagitta due to the mechanical mounting of the planes. We conclude that the long term operation of the Geiger tube system is satisfactory.

5.5.2. Flash chambers

Spark gaps are systematically replaced after one year of operation which corresponds to ~ 350 000 pulses. This is done once a month for ~ 100 of them during a 4 h shutdown of the experiment. This procedure was found most convenient as it minimizes the chance of spark gap failures although we known by experience that most spark gaps may operate properly twice as long.

With the flash chamber elements themselves we experienced until now the following failures:

(1) 33 of the 1824 hv delay lines developed a short circuit. All of them have been replaced by external capacitor banks with no loss to the detector.
(2) 36 out of 1824 FC elements developed a short circuit between the electrodes in a region inaccessible for repair.
(3) 34 of the 3648 polypropylene panels have developed a gas leak and have been taken out of the gas distribution system. Some of them have been reactivated with a reduced gas flow.

Overall, ~ 100 out of 3648 panels are inactive (3%). They are distributed randomly throughout the detector.

Apart from these failures, the detector properties have been stable. Therefore we consider the long term ageing of the detector as satisfactory.

6. Detector performance

The results on the properties of the Fréjus detector which are reported here have been obtained from data taken with the Fréjus detector itself and data from a test calorimeter which has been exposed to low energy beams of electrons, pions and protons.

6.1. Spatial and angular resolutions

The main aim of this experiment is to investigate nucleon decay with a good rejection of atmospheric neutrino induced interactions. In addition, we use the detector to search for cosmic-ray point sources and to study the cosmic-ray chemical composition. In order to utilize best the fine grain of our calorimeter, we tried to minimize the effect of alignment errors as much as possible. The position of the origin (cell #1) of each plane has been measured in the laboratory coordinate system. Also the detector distortions with respect to a perfect parallelepiped have been estimated using position measurements of the eight corners of the full detector and of alignment marks at both sides of each plane. The local distortions at any point inside the detector have been obtained by fits to parabolic functions of the x, y and z coordinates. As a final check, the results have been compared to straight line fits of long muon tracks. We found good agreement between the two methods.

6.1.1. Spatial resolution

Straight line fits of muon trajectories with little bremsstrahlung have also been used to measured the effective spatial resolution of the detector. If $x = az + b$ is the straight line equation fitting a track in one view, we calculate for each hit the perpendicular distance δ_i

$$\delta_i = \frac{x_i - (az_i + b)}{\sqrt{1 + a^2}}. \tag{4}$$

The rms deviation of the δ_i distribution (fig. 29) is $\sigma \sim 5$ mm, i.e. of the order of the cell dimensions. This is larger than the expectation on purely geometrical grounds for a perfect detector (1.5 mm) because, first, bremsstrahlung and delta rays induce a degradation of the residuals of the fit and, second, the local deformations deviate from the linear approximation. The fine grain resolution of the detector is illustrated in figs. 30a and b which show a multimuon event and a neutrino interaction respectively.

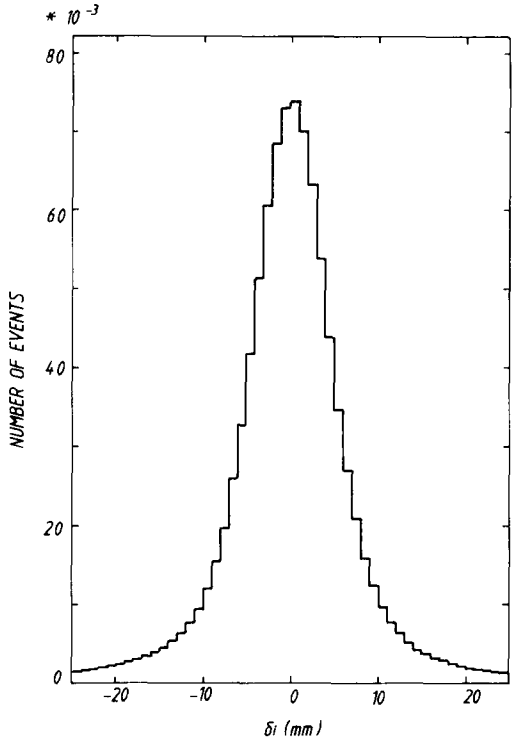

Fig. 29. Spatial resolution.

6.1.2. Angular resolution

The angular resolution of muon tracks from atmospheric bundles is given by the intrinsic detector resolution (due to the finite cell size of the detector) and by the multiple scattering in the rock above the laboratory. From a study of the nonparallelism of multimuon events in our detector we can extract the sum of both effects. We found an rms angular resolution of $\sigma_\theta = 1.0°$.

The intrinsic angular resolution can be studied separately by computing for each muon track the angle θ between the two directions obtained by linear fits to the first and second half sets of flash chamber tubes on each muon track. Using the rms width σ_θ of this angle, it is easy to show that the intrinsic angular resolution is $\sigma_\theta/\sqrt{8}$. The corresponding distribution is shown in fig. 31 which yields an intrinsic angular resolution of 0.4°.

6.2. Detector response to low energy particles

For the analysis of nucleon decay candidates in our detector an experimental study of the response to low energy particles is essential.

6.2.1. Description of the test detector

In order to investigate this response, we have built a

test detector which resembles the structure of the Fréjus detector as closely as possible. The test stack consisted of eight supermodules, each supermodule having an area of 70×70 cm^2 with 128×128 flash chamber channels. Each supermodule was supported by an individual iron structure. This arrangement allows us to position

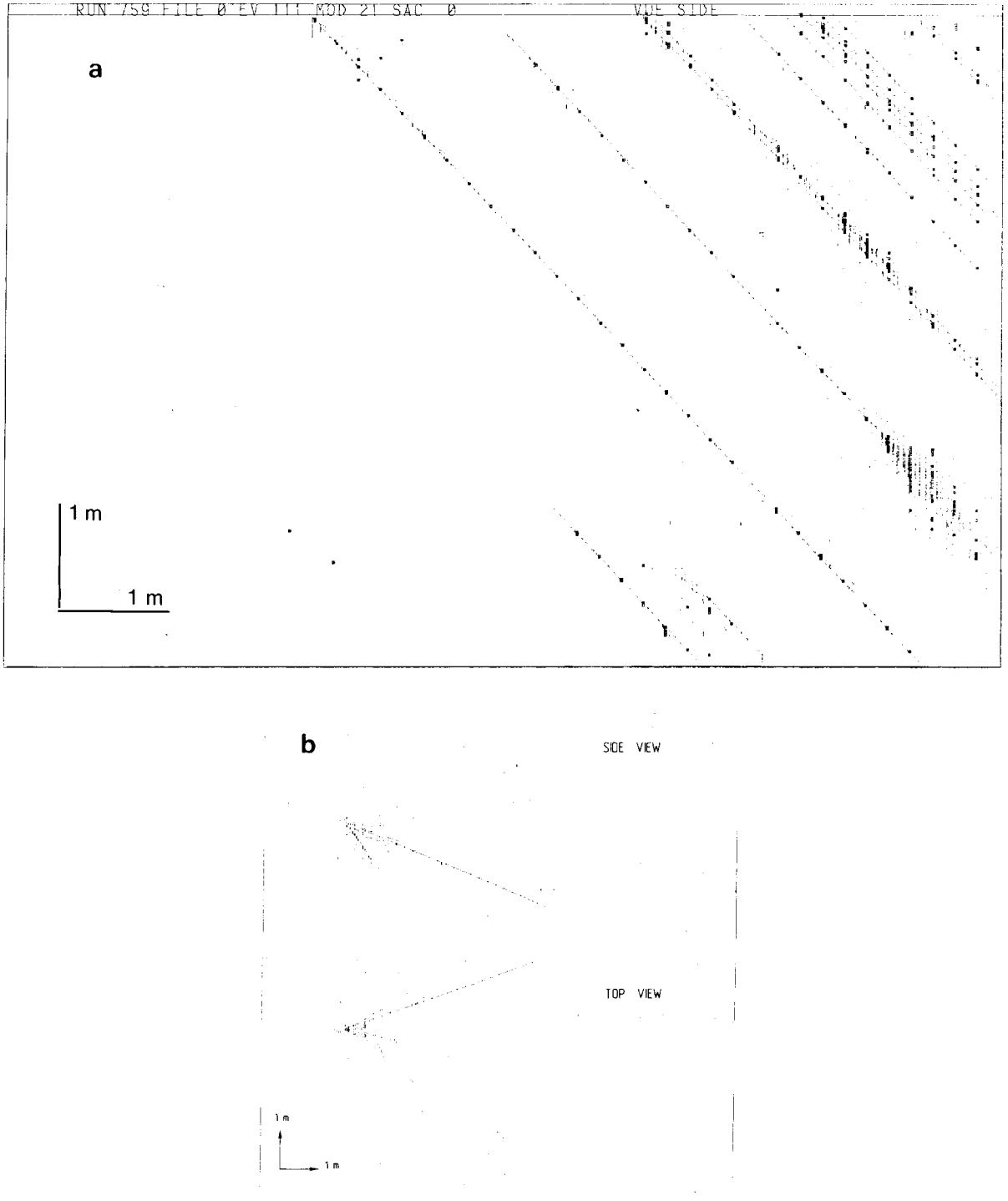

Fig. 30. (a) Multimuon event recorded in the Fréjus detector. (b) Charged current neutrino interaction. The visible energy is >10 GeV.

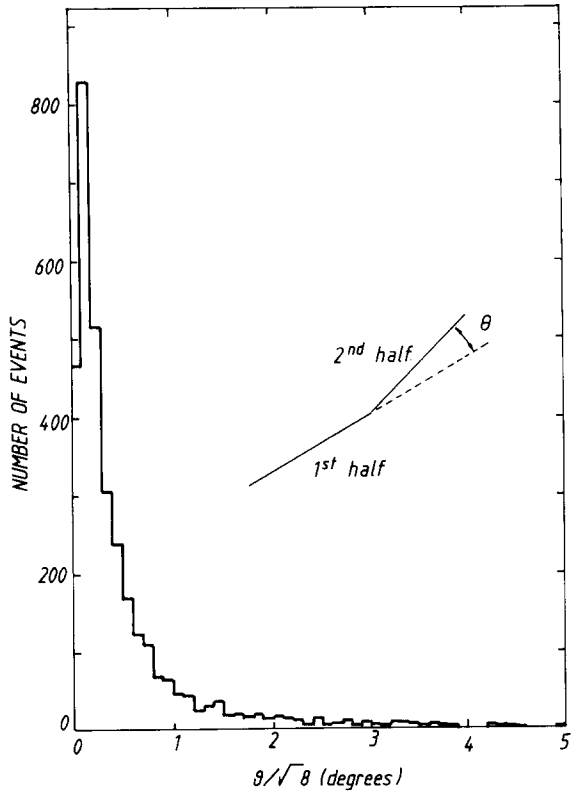

Fig. 31. Angular resolution.

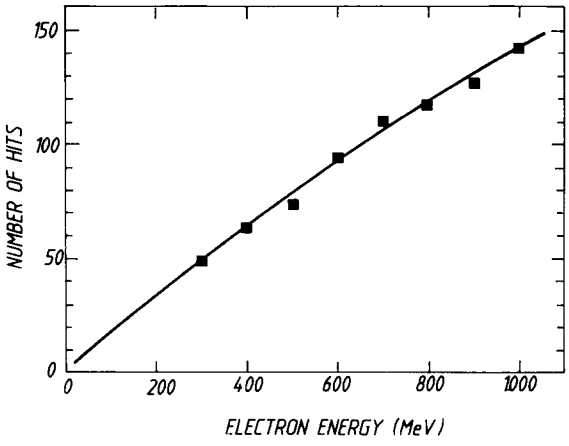

Fig. 32. Electron energy calibration.

the detector at different angles with respect to the beam. The flash chamber elements were equipped with the same high voltage and readout electronics as used in the Fréjus detector. The built-in Geiger tube elements were not equipped with electronics, because we used a trigger provided by scintillation counters and proportional chambers in the test beams. We exposed the test detector to an electron beam with momenta from 250 up to 6000 meV/c at the Deutsches Elektronen Synchrotron (DESY, Hamburg) and to a beam of photoproduced pions and protons with momenta ranging from 200 to 700 MeV/c at the electron synchrotron of the Bonn University.

6.2.2. Electrons

In fig. 32 the number of test detector cells fired by particles of the shower is plotted versus the energy of the incoming electron. Between 300 and 800 MeV the detector response is nearly linear with a slope of roughly 140 hits/GeV. At higher energies (> 1000 MeV, not shown in the figure) saturation effects set in. We used the EGS Monte Carlo code [24] with a special treatment of very low energy particles to simulate electromagnetic showers in the test detector in the wide energy range from 300 MeV to 6 GeV. We found very good agreement between data and Monte Carlo calculation not only for the calibration but also in much more detailed features of the shower topology. We are therefore confident that we can use the Monte Carlo results also below 300 MeV where no test data are available. The number of fired cells $N(E)$ as a function of the electron energy E can be fitted by a simple form (see solid line in fig. 32):

$$N(E) = A_1 E/\left(1 + A_2\sqrt{E}\right), \tag{5}$$

with $A_1 = 205$ GeV^{-1} and $A_2 = 0.44$ GeV$^{-1/2}$ in the energy interval [0,1] GeV for electrons perpendicular to the detector planes. The energy resolution is basically determined by the fluctuation of the number of hits at a given energy. Because of the saturation effect we cannot expect a simple $1/\sqrt{E}$ behavior. We found, however, that the resolution is described with an accuracy of about 10% by the two-term formula

$$\sigma_E/E = 0.055 + 0.06/\sqrt{E}\,, \tag{6}$$

for E above 0.3 GeV. The transfer of these results to the Fréjus detector is straightforward only if the efficiencies are the same in both detectors. In case of unequal efficiencies, the correction factor is not a simple constant because in the core of a shower one can have multiple hits in one cell. Even more important is the study of showers which are not perpendicular to the iron plates of the detector, in which case $N(E)$ is somewhat smaller. Both problems are solved with the help of the EGS Monte Carlo code using parameters which have been adjusted to the test detector data. In fig. 33 we show as an example the multiplicative correction factor for $N(E)$ as a function of θ in the xz plane ($\theta = 90°$ is for showers perpendicular to the plates).

6.2.3. Photons, π^0

Because we did not have access to a low energy tagged photon beam, we investigated the response to photons using the charge exchange reaction $\pi^- +$ nucleus $\rightarrow \pi^0 +$ anything.

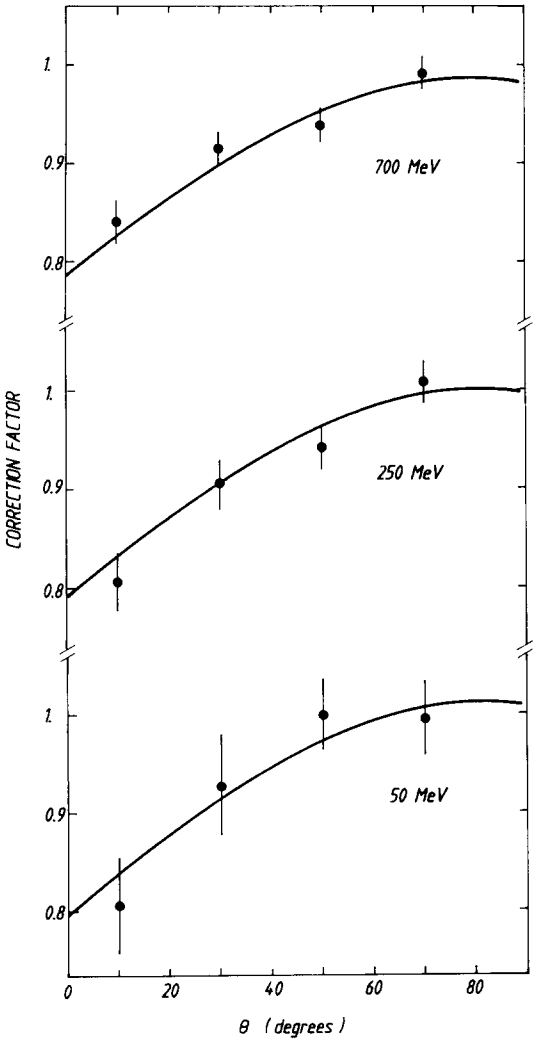

Fig. 33. Correction factor to the energy response as a function of the angle of incidence to the detector planes.

We visually scanned 11 348 events from the Bonn test run and found 126 clear candidates for this reaction. The only free parameter in the reconstruction of the invariant mass (see fig. 34) was a calibration factor. The photons had energies ranging from 60 to 350 MeV. The fitted calibration constant for photons agreed within errors with the average slope given by eq. (5) for low energy electrons. This simple result is also supported by the EGS Monte Carlo code, which showed that a 200 MeV photon produces in our detector the same number of hits as an electron of the same energy. The average reconstruction efficiency for π^0's produced isotropically is $\sim 50\%$ for $p_\pi = 250$ MeV/c and goes up to 60% for $p_\pi = 600$ MeV/c. Thus our detector is well suited for the reconstruction of nucleon decay channels with neutral pions in the final state.

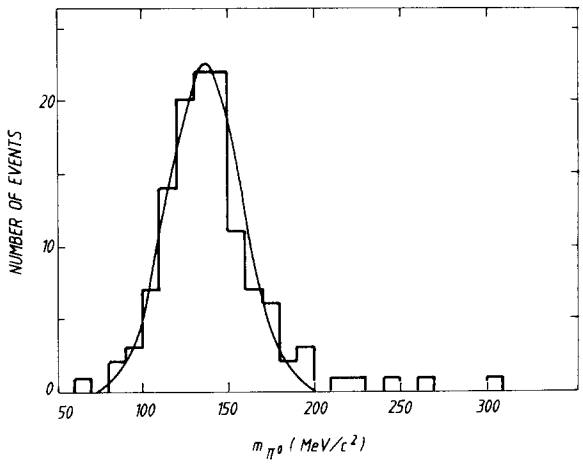

Fig. 34. Reconstructed π^0 mass in the test detector.

6.2.4. Charged pions

The photoproduced pions at the Bonn synchrotron traversed a system of scintillation counters and an analyzing magnet before hitting the test detector. A beam momentum resolution of $\sigma_p/p \sim 8\%$ was achieved. Most of the low energy pions show up in our detector as "straight lines" with some multiple scattering. Using a simple track finding algorithm we determined for each track the material thickness traversed. The experimental range distributions show that for momenta above 400 MeV/c only a small percentage of pions stop within 10% of the nominal "Bethe–Bloch range".

The detector response to low energy pions has also been simulated with the GEISHA Monte Carlo code [25] including a full description of the detector (cell structure, efficiencies etc.). In fig. 35a the experimental range distribution is compared with the Monte Carlo calculation. Because a good agreement also holds for higher momenta, we conclude that we can use the Monte Carlo code to extrapolate to zero-momentum spread. This is shown in fig. 35b for a nominal momentum of 300 MeV/c. Our findings agree with previously published results on pion range measurements [26].

6.2.5. Muons

The energy of fully contained muons is obtained from their range by standard range–momentum relations which take into account the various materials crossed by the particle. Below 500 MeV/c, the main uncertainty in the momentum determination comes from the intrinsic error made in the evaluation of the range. The average value of this error is ± 3.5 g cm^{-2}/cos θ, where θ is the angle between the particle trajectory and the normal to the detector planes. The total error Δp_μ is calculated by adding quadratically the error of the range and the straggling contribution [27]. In fig. 36, Δp_μ is plotted as a function of momentum for three angles of incidence θ.

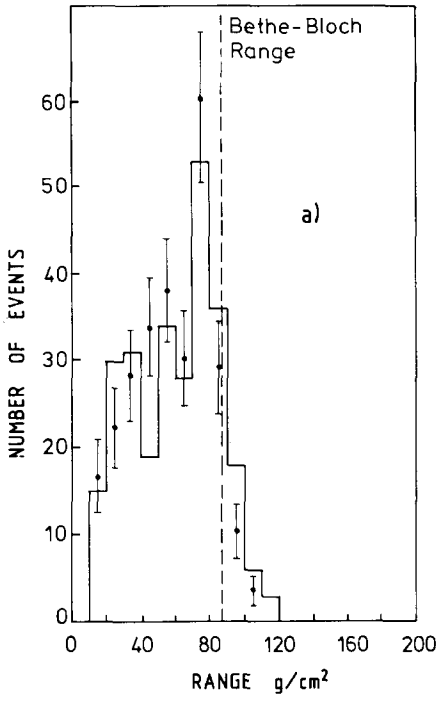

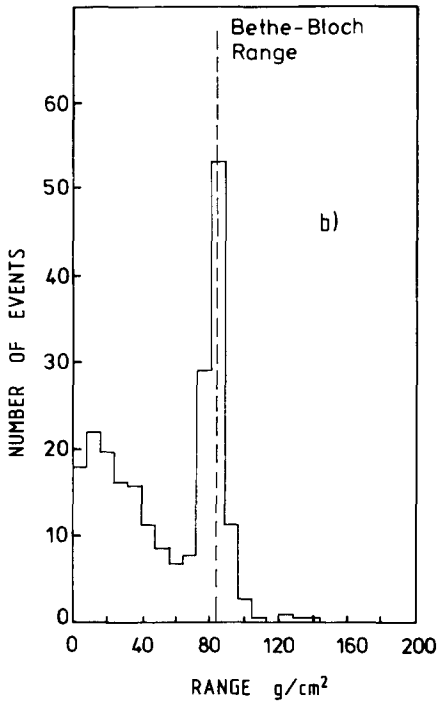

Fig. 35. Range distributions for 300 MeV/c negative pions: (a) Data points are from the test detector. The histogram shows Monte Carlo results for a 20% fwhm momentum spread. (b) Monte Carlo range distribution for zero momentum spread.

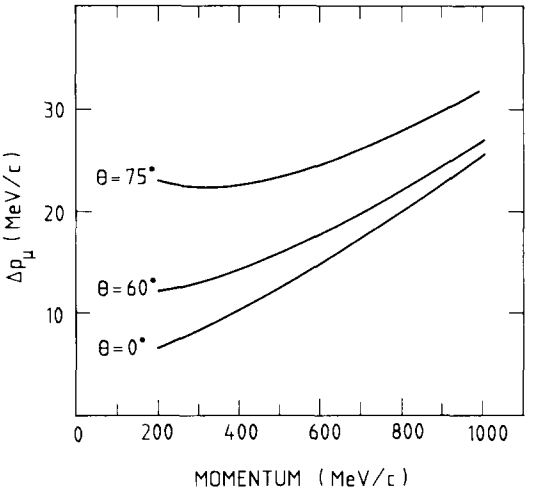

Fig. 36. Average uncertainty of the muon momentum determined by range.

6.3. *Particle identification*

6.3.1. *e, γ versus μ, π*

Due to the fine grain of our calorimeter, it is easy to separate showers from single ionizing tracks down to low energies using the very different topologies of showers and ionizing tracks. As a rule of thumb, the number of hits in the test detector per traversed plane is 1.2 for pions and muons and at least 2.0 for showers with energies above 200 MeV.

6.3.2. *e–γ separation*

If the vertex is known, we can distinguish between photon and electron showers. We have measured the conversion length experimentally using our π^0 data. The result shown in fig. 37 agrees with the values in the literature [28]. Electrons in our detector also have an artificial conversion length because the flash cell efficiency is not 100%. For electrons with perpendicular incidence, this length is 0.5 cm. Defining the photons to be showers with the first hit at least 1.5 cm after the vertex, we can identify typically 90% of the photons and electrons correctly. The application of these results to other geometrical conditions is straightforward since the conversion length is roughly proportional to the radiation length.

6.3.3. *π–μ separation*

It is very hard to distinguish in our detector low energy pions from muons using only topological criteria. Demanding a secondary track to have at least 3 hits, only 0.5% of the test detector events have a visible inelasticity. In our detector the occurrence of visible kinks, recoils or stars is only of the order of a few percent and thus cannot be used to efficiently distinguish muons from pions.

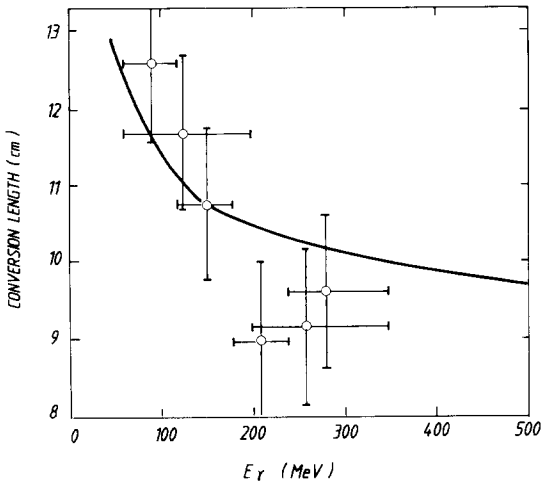

Fig. 37. Conversion length for γ's coming from the π^0 sample.

6.4. Event topology improvement with Geiger pulse timing

For the complete detector (113 Geiger planes, ~ 40 000 tubes) the average experimental number of 20 spurious Geiger tube hits read out with each event is in good agreement with the expected value as calculated from the singles rate per plane and the average Geiger pulse length of 60 μs. An isolated Geiger hit can be eliminated if it is not in time as indicated by the timing system and also in the trigger configuration data. The number of spurious hits left per event is $20 \times (0.4\ \mu s/60\ \mu s) = 0.15$. Distributed in the 440 m^3 volume of the detector, its probability to contaminate the ~ 1 m^3 volume of a typical nucleon decay event is negligible. Thus, after analysis, only Geiger hits belonging to the event remain.

The topology of an event is mainly determined with the flash chamber hits. However, since the less densely distributed Geiger tube hits all belong to the event, they may confirm doubtful flash chambers hits, thus improving the event topology.

7. Conclusion

The Fréjus detector is the largest underground tracking calorimeter with the finest ganularity presently working. It has been taking data for more than three years. The acquisition time amounts, mid-1987, to about 900 live days and corresponds to a sensitivity, for the total detector volume, of 1.9 kt yr. The performance of the detector has been studied with atmospheric muons in the Fréjus laboratory and with a test detector exposed to electron and pion beams. Results are compatible with expectations.

Acknowledgements

We are most grateful to A. Rousset for his unfailing support of the project when it was in its initial phase. The late Ph. Delcros greatly contributed to the construction of the laboratory. We also thank F. Jacquet and M. Reposeur for their assistance. Thanks are due to the French and Italian authorities of the Fréjus tunnel, SFTRF and CITAF, for their collaboration.

We are very grateful to P. Prugne whose support in the flash chamber construction was essential. Special mention should be given to S. Henry, M. Kalifa and Ch. Wannepain for their dedicated work during the testing of the flash chamber elements. We thank J.C. Brisson who designed the readout electronics for these tests.

Finally we thank the Physikalisches Institut der Universität Bonn and the Deutsches Elektronen Synchrotron (DESY) Hamburg for the use of their test beam facilities.

References

[1] P. Bareyre et al., Proposition d'une expérience pour l'étude de l'instabilité du nucléon au moyen d'un détecteur calorimétrique (1980) unpublished.
[2] A. Rousset, Ph. Delcros, M. Levy and J.M. Demorieux, TRAVAUX (février 1983) p. 9.
[3] M. Conversi and A. Gozzini, Nuovo Cim. 2 (1955) 189; M. Conversi and L. Federici, Nucl. Instr. and Meth. 151 (1978) 93.
[4] F.E. Taylor et al., IEEE Trans. Nucl. Sci. NS-27 (1980) 30; D. Bogert et al., IEEE Trans. Nucl. Sci. NS-29 (1982) 363.
[5] R.C. Allen et al., IEEE Trans. Nucl. Sci. NS-28 (1981) 487.
[6] Beghin-Say, Division AKILUX, Kunheim, 68 Kaysersberg, France.
[7] Nieff, 213 av. de la Pressence, 69200 Venissieux, France.
[8] J. Thierjung, Diplomarbeit, Univ. Wuppertal, No. WUP B80/10.
[9] A. Baracat, J. Heitzmann and Y. Laigneau, Internal Report 85-019 (1985) DPhPE-STIPE Saclay.
[10] Montedison France, Tour Franklin-Cedex 11, 92081 Paris La Defense.
[11] R.A. Smythe et al., Nucl. Instr. and Meth. 193 (1982) 457 and ref. therein.
[12] Automate Syclop, Mecilec, France.
[13] Linit 10, Sulzer Bros (UK), Blackwater way, Aldershot Hampshire GU12 4DR, UK.
[14] Packard Instruments GmbH, Model 437.
[15] Bulten–Kanthal, BP no. 38, 92704 Colombes Cedex, France.
[16] B. Kuznik, Diplomarbeit, Univ. Wuppertal, no. WUP D82/11; E. Coulareau, Internal Report DPhPE-STIPE Saclay, STD002 (1987).
[17] ATNE, av. de l'Atlantique Z.A. Courtaboeuf, 91940 Les Ulis.

[18] Hydrogen Thyratron, F103 ITT, 38 av. Henri Barbusse, 92220 Bagneux, France.
[19] B. Dudelzak et al., Nucl. Instr. and Meth. 222 (1984) 436.
[20] Ph. Hubert et al., Mesure des taux de radioactivité naturelle pour les matériaux du détecteur τ_p, Rapport Interne CERNBG 8539.
[21] E. Barrelet et al., Proc. Topical Conf. on the application of microprocessors to high energy physics (1981).
[22] IEEE STD 488-1975, Standard Digital Interface for Programmable Instrumentation, IEEE Instrumentation and Measurement Group.
[23] D.L. Edmunds et al., Nucl. Instr. and Meth. 192 (1982) 325.
[24] R.L. Ford and W.P. Nelson, SLAC Report 210 (1978).
[25] H. Fesefeldt, GEISHA Version 7.U, Aachen Preprint PITHA 85/02.
[26] J. Augustin et al., Nucl. Instr. and Meth. 36 (1965) 213.
[27] R.M. Sternheimer, Phys. Rev. 117 (1960) 485.
[28] J. Hubbel et al., J. Phys. Chem. Ref. Data 9 (1980).